2017

Computational Approach to Electrocatalysis

Nagendra Dhakal
University of Central Florida

COMPUTATIONAL APPROACH TO ELECTROCATALYSIS

by

NAGENDRA DHAKAL
B.S. Physics, Tribhuvan University, Nepal, 2002
M.S. Physics, University of Southern Mississippi, 2008

A dissertation submitted in partial fulfillment of the requirements
for the degree of Doctor of Philosophy
in the Department of Physics
in the College of Science
at the University of Central Florida
Orlando, Florida

Spring Term
2017

Major Professor: Sergey Stolbov

ABSTRACT

The main objective of this work is to understand the theoretical basis of the working principle of the Hydrogen fuel cell. We seek the physical basis of the Rational Design Technique, the smart way of preselecting materials from the material-pool, implemented in our study anticipating highly promising electrocatalysts for promoting the conversion of chemical energy stored in hydrogen molecules into the electrical energy. It needs the understanding of the relationship among the compositions of the materials under consideration, their electronic structure and catalytic activities. We performed the first principle DFT calculations to achieve the goal.

Our work is focused first on the issues in hydrogen oxidation reaction taking place in anode compartment of the cell. Next comes up with the issues with Oxygen Reduction Reaction taking place in cathode compartment. Finally, we focus on mechanisms underlying binding of small molecules on substrates.

Platinum perfectly catalyzes hydrogen oxidation reaction on the hydrogen fuel cell anodes. However, it has at least two drawbacks: a) it is too expensive; b) it has a low tolerance to CO poisoning. Pt-Ru bi-functional catalysts are more tolerant to CO, but they are still very expensive. In this work, we performed first-principle studies of stability and reactivity of M/W (110) structures, where M = Pd, Ru, Au monolayers. All three systems are found to be stable: formation energy of MLs is significantly higher than cohesive energy of the M-elements. The calculated binding energies of H, H_2, OH, CO, and H_2O were used to obtain the reaction free energies. Analysis of the free energies suggests that Au-W bonding does not activate sufficiently Au monolayer, whereas Ru/W (110) is still

too reactive for the CO removal. Meanwhile, Pd/W (110) is found to catalyze hydrogen oxidation and at the same time to be highly tolerant to the CO poisoning. The latter finding is explained by the fact that CO binds much weaker to Pd on W (110) than to Pt, while the OH binding is strong enough to ensure CO oxidation. The obtained results are traced to the electronic structure of the systems.

Oxygen Reduction Reaction (ORR) is the heart core reaction in fuel cells, Proton Exchange Membrane Fuel cell and DEMFC. However, the reaction is not so obvious and need suitable electrocatalyst. Pt or Pt-based catalysts are found to be the best catalyst so far. But, its cost and shortage make it not feasible economically. Moreover, lower onset potential (maximal electrode potential at which the reaction can proceed) of such catalysts is offering another limitation to fuel cell performance. Research has been conducted in many directions for lowering the cost by replacing the Pt with some other elements of lower cost or reducing the Pt-load in the material; and even more finding the material performing better than Pt. In this paper, we've tried to understand the ORR mechanism and look for the material that could be potential option to Pt. Our calculations suggest that for monolayer of Pt on 5 layered slab of Nb or Mo the onset potential is the same as for Pt, while cost of these systems are much lower than that of Pt. Presence of water changes the reaction rate very minimum. Rational design method facilitates the research of selecting the appropriate catalyst and saves time and effort significantly. The result shows that the d-band center model is not accurate to describe the reactivity of the catalyst.

For decades, adsorbates' binding energy (E_B) has been used as an indicator of the adsorbate-substrate bond strength (E_{BF}). Thus, although one can compute accurately any E

models to gauge bond-strength are developed and applied to rationalize and anticipate E_B's because that is a key aspect in the rational search for efficient catalysts. Yet bond-strength alone fails to predict E_B trends. Therefore, quantifying and understanding the difference between E_B and E_{BF} is essential to catalysts design. Indeed, the adsorbate-substrate bond formation perturbs the substrate's electronic charge density, which reduces E_B by the energy attached to such perturbation: E_{pert}. Here, with the example of carbon monoxide adsorption on metal-doped graphene, we show that $Epert$ may exceed 1 eV and render an unusual situation: although the E_B of CO to the Au-doped graphene indicates that binding does not happen, we find evidence of a strong bond between CO and the substrate. Thus, in this case, the large E_{pert} totally disrupt the equivalency between E_{BF} and E_B we also propose a method to compute E_{pert} that bypasses dealing with an excited electronic state of the system.

ACKNOWLEDGMENTS

I would like to thank my advisor Dr. **Sergey Stolbov** for his constant encouragement, advisement and guidance during my Ph.D. I am so grateful to Dr. **Talat S.Rahman** and her group for the thoughtful discussion. I would remember Dr. Rahman not only as a professor but as a guardian, as a parent. Special thanks goes to Dr. **Madhab Neupane** and group for encouragement and inspiration. I am grateful to all my professors and dear staff in the department of physics. I, specifically, would like to express sincere thanks to Dr. **Marisole Ortigoza** for her valuable suggestions and discussions in developing the projects in form.

I do have a sincere gratitude to all Professors in my graduate committee, **Dr. Sergey Stolbov, Dr. Talat Rahman, Dr.Masahiro Ishigami** and **Dr. Artem Masunov**, for providing valuable time and suggestions in completing my dissertation.

I cannot stay without thanking all colleagues that I had a discussion with in developing ideas in carrying on the research. All well-wishers and my relatives especially my wife and little kids who killed their desire of seeing me in day time in front are always in mind. I cannot forget the support that I got from my teachers starting from my primary school and all helping hands in my way until now.

Also, I would like to thank the UCF EXCEL program and the Physics Department for the financial support. I appreciate and thank SOKES for providing me access and space for running my jobs in the cluster.

TABLE OF CONTENTS

LIST OF FIGURES

LIST OF TABLES

CHAPTER 1 INTRODUCTION

1.1 Preamble

Since people started noticing the mystery and perfection of nature, they stared thinking about the reasoning behind it, they tried to explore and understand the secret behind it. In early ages people had a needle and the plate of sand to visualize what they observed and argued. Pen and papers came after a long time to jot down their views. Mathematical equations emerged there to comply with their ideas and to model the problems. It took a long time to come up with the complete set of such equations to handle the real problems. Basically, people had to deal with the many body problems consisting of very tiny particles, i.e. atoms and sub atomic particles. In the meantime, the biggest gift of 20^{th} century, computer provided a big leap to theoretical study of the systems, the computational physics.

1.2 Motivation:

Energy has been an indispensable aspect of today's world. Major sources of energy at present are limited as they are no-renewable and the world is going to have energy crisis in future. New and reliable sources of energy have been the main goal of many research topics today. Studies have been done in finding the ways to minimize the consumption of energy as well. Some sources are taken to be reliable and good alternative to the present energy solution, however, they need more focus to make them better and applicable. Solar cell, fuel cell are some of the examples. This research is focused on some important aspects of the fuel cell and we've tried to contribute to improve it.

Personal interest begins a bit differently. As a curious child, I used to think and play with the tools available around to make little stuffs, such as a little water mill and so on. Near my final of Grade 10, the SLC [Iron Door], the atmosphere was filled with a big political movement in my homeland. Somehow, the boarder was blocked and the only intake route was closed. We did not have electric power and had to use kerosene lamp to read at night. But the blockage shut everything down, I was very upset on that. I collected some broken pieces of mirrors and made moon light focus on my books to read. It went for a while. I started thinking of a source of the energy that can never be blocked by anyone!! I was convinced it to be solar energy. I started dreaming zero energy houses, zero energy transportation and so on. I made a solar battery by using a copper vessel, silver plate and copper oxide. It proved me that we can make solar cells. In M.Sc. thesis, I studied thermal process of solar energy. Solar air heaters were modeled, designed and one of them was fabricated. At the end, I came to go with the fuel cell as my Ph.D. research.

1.3 **Direct conversion of Chemical energy to Electricity: Fuel Cell.**

Fuel cell is a device to convert chemical energy stored in hydrogen molecule directly into the electrical energy. There are different types of fuel cells under study and in practice as well. Proton Exchange Membrane Fuel Cell [PEMFC] is one of them that consists of the Proton Exchange Membrane [PEM] as an Electrolyte. However, the basic working principle is the same for all where Hydrogen and Oxygen molecules are made to react (opposite of electrolysis of water). The most simple and common reaction encountered in fuel cells is [1]

$$H_2 + \frac{1}{2} O_2 \rightarrow H_2O \quad (1.3.1)$$

The whole reaction can be divided in to two half equations occurring in two compartments of the cell. Hydrogen molecule is fed through the anode compartment that dissociates into hydrogen ion (H^+) and electron (e^-). This reaction is called Hydrogen Oxidation Reaction [HOR].

$$H_2 \rightarrow 2H^+ + 2e^- \quad (1.3.2)$$

The H-ion migrates through the Proton Exchange Membrane and the free electron goes through the external circuit constituting a current. At the same time the oxygen molecule adsorbed in the cathode compartment undergoes dissociation by accepting electron and combine with Hydrogen Ion. This reaction is called Oxygen Reduction Reaction [ORR].

$$\frac{1}{2} O_2 + 2H^+ + 2e^- \rightarrow H_2O \quad (1.3.3)$$

Thus, in fuel cell Hydrogen and Oxygen fuse to give out water with the generation electricity. So, it is one of the cleanest means of generation of electricity. Figure below gives the schematic action of the Fuel cell:

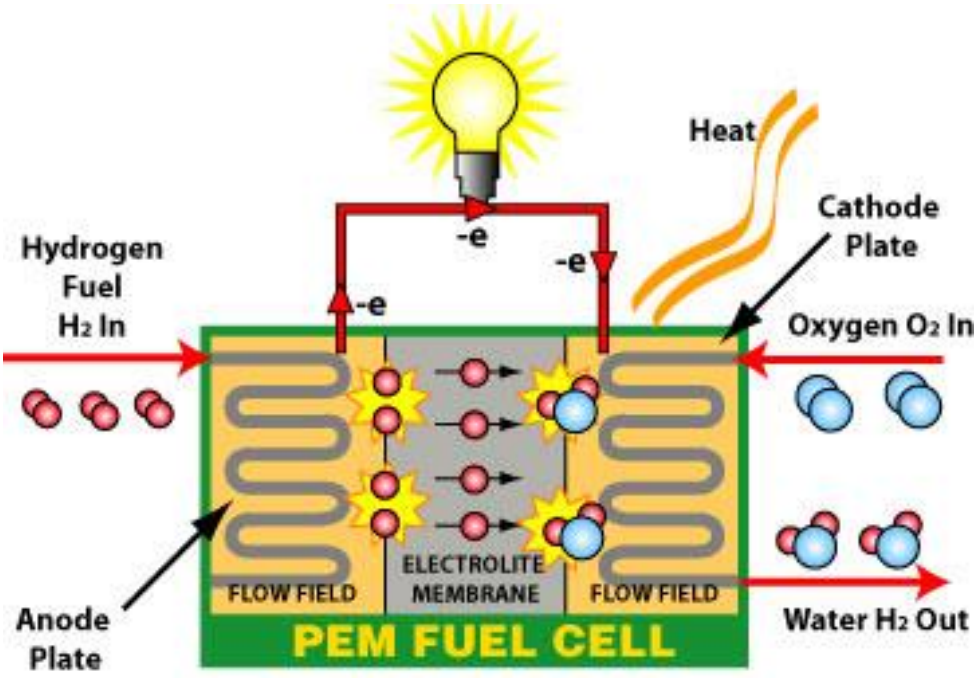

Figure 1: Schematic diagram showing the action of Fuel Cell.[2]

The reactions in either compartments, however, are not obvious (dissociation of H_2 in anode electrode is not easy and the reaction in cathode, ORR is too slow) and need catalysts to carry them up. Platinum has been the best in the pool of the elements available so far for both anode and cathode reactions. However, because of its low availability and high cost it has been offering an unacceptably high price to fuel cell for its commercialization. Moreover, there are some obstacles in its action as a catalyst that put the limit to the performance of fuel cell too. Platinum is very reactive to CO that comes with H_2 intake. CO binds on Pt stronger which occupies the active sites of Pt that are used for the H_2 dissociation in anode compartment. The poisoning effect of CO on Pt is one of the major issues to be addressed. Cathode electrode is in acidic environment. The stability of Pt in

cathode electrode, has thus been a serious issue to be pointed out. Relatively low onset potential puts the limit to the performance of fuel cell and hence the efficiency.

Studies have been conducted to minimize the cost and optimize the activity of the catalyst. First, way in this direction is to reduce the loading of Pt in the system under consideration. And the next is to search for the materials that could replace Pt and perform better.

Some research has been done with the monolayer on a slab, nanoparticles as well.

1.4 **Outline of Thesis**

The purpose of this thesis is to study and analyze the important aspects of the electrocatalysis that are applicable to fuel cell. There are several factors controlling the reactivity of the materials. It's a challenge in finding the appropriate electrocatalyst since it has to show weak reacting to some adsorbates while strong to some others. In our study, we follow the ways of tuning the electrocatalytic properties and it is based on the Rational Design Principle. Meanwhile, we dig in to the mechanism of the binding of an adsorbate in a surface and the validity of the well-known and well established relation of binding energy and stability; bond formation energy and binding. Our result obtained from the first principle are discussed in chapter 3, 4 and 5. Chapter 2 gives the theoretical overview.

In chapter 3, we present our result on poisoning effect of CO on the catalyst. Platinum perfectly catalyzes hydrogen oxidation reaction on the hydrogen fuel cell anodes, but it has a low tolerance to CO poisoning. Currently hydrogen is mostly produced from natural gas. One of the reaction product is CO. It is very hard and expensive to purify hydrogen. The CO molecules remaining in the gas even after purification adsorb to the anode catalyst and

this way block the reaction active sites and thus reduce the reaction rate. Presence of water on the anode leads to creation some fraction of OH radicals which can react with CO making CO_2 that is easy to remove. To make this reaction favorable one needs to achieve a controversial condition: CO has to bind weakly to the catalyst, whereas the catalyst has to be reactive enough to produce enough OH from water. In this work, we performed first-principle studies of stability and reactivity of M/W (110) structures, where M = Pd, Ru, Au monolayers. All three systems are found to be stable: formation energy of MLs is significantly higher than cohesive energy of the M-elements. The calculated binding energies of H, H_2, OH, CO, and H_2O were used to obtain the reaction free energies. Analysis of the free energies suggests that Au-W bonding does not activate sufficiently Au monolayer, whereas Ru/W(110) is still too reactive for the CO removal. Meanwhile, Pd/W (110) is found to catalyze hydrogen oxidation and at the same time to be highly tolerant to the CO poisoning. The latter finding is explained by the fact that CO binds much weaker to Pd on W(110) than to Pt, while the OH binding energy is strong enough to ensure CO oxidation. The obtained results are traced to the electronic structure of the systems.

In chapter 4, we present the action of catalyst in ORR taking place in cathode compartment. Oxygen Reduction Reaction (ORR) is the heart core reaction in fuel cells, Proton Exchange Membrane Fuel cell and DEMFC. However, the reaction is not so obvious and need suitable electrocatalyst. Pt or Pt-based catalysts are found to be the best catalyst so far. But, its cost and shortage make it not feasible economically. Moreover, relatively low onset potential of such catalysts is offering another limitation to fuel cell performance. Research has been conducted in many directions for lowering the cost by

replacing the Pt with some other elements of lower cost or reducing the Pt-content in the material; and even more finding the material performing better than Pt. In this paper, we've tried to understand the ORR mechanism and look for the material that could be potential option to Pt. We've found that monolayer of Pd on Nb or Mo being much less expensive than Pt have the onset potential of ORR the same as Pt does. Presence of water changes the reaction rate very minimum. Rational design method facilitates the research of selecting the appropriate catalyst and saves time and effort significantly. The result shows that the d-band center model is not accurate to describe the reactivity of the catalyst.

In chapter 5, we present our result that we got from our calculation that is raising the questions about the well-known concept of adsorbate binding. For decades, adsorbates' binding energy (E_B) has been used as an indicator of the adsorbate–substrate bond strength (E_{BF}). Thus, although one can compute accurately any E_B models to gauge bond-strength are developed and applied to rationalize and anticipate E_B's because that is a key aspect in the rational search for efficient catalysts. Yet bond-strength alone fails to predict E_B trends. Therefore, quantifying and understanding the difference between E_B and E_{BF} is essential to catalysts design. Indeed, the adsorbate-substrate bond formation perturbs to the substrate's electronic charge density, which reduces E_B by the energy attached to such perturbation: E_{pert}. Here, with the example of carbon monoxide adsorption on metal-doped graphene, we show that E_{pert} may exceed 1 eV and render an unusual situation: although the E_B of CO to the Au-doped graphene indicates that binding does not happen, we find evidence of a strong bond between CO and the substrate. Thus, in this case, the large E_{pert}

totally *disrupt the equivalency between E_{BF} and E_B* we also propose a method to compute E_{pert} that bypasses dealing with an excited electronic state of the system.

CHAPTER 2
THEPRITICAL BACKGROUND

2.1 Introduction

This chapter presents the theoretical backbone that the dissertation is founded. It begins with addressing the challenges in understanding the realistic systems and developing right form of mathematical equation expressing them. The properties of matter are determined by the interaction of electrons and atomic nuclei and hence the quantitative theoretical description of the solid state system starts with stating quantum many body problems ruled by Schrödinger equation. It turns out to be a complex coupled differential equation with many degrees of freedom. This chapter begins with development of the Hamiltonian describing many particles in condensed matter and is followed by the sections describing the ways of solving the complex equation.

2.2 Many Body Problem

Most of the properties of materials are determined by the behavior of the valence electron and those near the nucleus form a closed shell and are expected to have a minimal effect. The valence electrons essentially are quantum systems that can be described with quantum mechanical techniques. The electronic states can be found as a solution of the Schrödinger equation:

$$\hat{\mathcal{H}}\Psi = E\Psi \tag{2.2.4}$$

Where E is the eigenvalue and Ψ is the eigenstate. Then Hamiltonian describing the system of the particles takes the general form of

$$\mathcal{H} = T_I + T_e + V_{II}(R_I) + V_{e-e}(x_i) + V_{e-I}(x_i, R_I), \qquad x_i = r_i, \sigma_i \quad (2.2.5)$$

$$\mathcal{H} = -\frac{\hbar^2}{2}\sum_{I=1}^{M}\frac{\nabla_I^2}{2M_I} - \frac{\hbar^2}{2m}\sum_{i=1}^{N}\nabla_i^2 + \frac{1}{2}\frac{e^2}{4\pi\varepsilon_o}\sum_{I\neq J}^{M}\frac{Z_I Z_J}{|R_I - R_J|} + \frac{1}{2}\frac{e^2}{4\pi\varepsilon_o}\sum_{i\neq j}^{N,N}\frac{1}{|r_i - r_j|} - \frac{e^2}{4\pi\varepsilon_o}\sum_{i,I}^{N,M}\frac{Z_I}{|R_I - r_i|} \quad (2.2.6)$$

Where, $M_I, R_I \; and \; Z_I$ represent mass, position and charge of M different ions and m, $r_i$and e are those of valence electrons respectively; and σ_i, the spin of i[th] electron. Here we discard the relativistic effect in e-e interaction and assumed that the spineless nuclei do not come close so as to overlap, the Frozen Approximation[3].

The Schrödinger equation with this Hamiltonian is a partial differential equation with (3N+3M) coupled degrees of freedom which would not be easily decoupled. It has been solved analytically only for simplest atom, the Hydrogen. For other systems based on the surface or other structures which includes many electrons and ions, the complete solution is impossible to obtain. So, approximations are needed to simplify the problem without losing the nature of problem.

2.3 **Separation of Electron and Lattice Variables:**

First step on simplifying the equation would be treating the problematic term in the equation, V_{e-I}that brings up electrons and ions together into the consideration. Based upon

the fact that the lighter electrons move very fast compared to the heavy nucleus in a system **Born-Oppenheimer Approximation[4]** suggests that electronic states (electron cloud) are able to adjust themselves rapidly to any change in nuclear coordinates, while staying in the ground state. This allows us to decouple the total wave function into electronic and the ionic components and write it as a product of the two. This is also called **adiabatic approximation.**

This can be exploited by assuming the quasi-separable ansatz of the form,

$$\Psi(R,r) = \sum_{\nu} \Lambda_{\nu}(R)\, \Phi_{\nu}(R,r) \tag{2.3.7}$$

Where $\Lambda_{\nu}(R)$ are the wave functions of nucleus of and $\Phi_{\nu}(R,r)$are the electronic wave functions, the Eigen states of the respective time independent Schrödinger equations.

More explicitly, we obtain the decoupled Schrödinger equations for the ions system as

$$H_I \Lambda_{\nu}(R) = E(\mathrm{R})\Lambda_{\nu}(R) \tag{2.3.8}$$

With

$$H_I = -\frac{\hbar^2}{2}\sum_{I=1}^{M}\frac{\nabla_I^2}{2M_I} + \frac{1}{2}\frac{e^2}{4\pi\varepsilon_o}\sum_{I\neq J}^{M}\frac{Z_I Z_J}{|R_I - R_J|} + \varepsilon_n(R) \tag{2.3.9}$$

And the electron system as

$$H_e\, \Phi_{\nu}(r,R) = \varepsilon_n(R)\, \Phi_{\nu}(r,R) \tag{2.3.10}$$

With Hamiltonian of electron,

$$H_e = -\frac{\hbar^2}{2m}\sum_{i=1}^{N}\nabla_i^2 - \frac{e^2}{4\pi\varepsilon_o}\sum_{i,I}^{N,M}\frac{Z_I}{|R_I - r_i|} + \frac{1}{2}\frac{e^2}{4\pi\varepsilon_o}\sum_{i\neq j}^{N,N}\frac{1}{|r_i - r_j|} \tag{2.3.11}$$

The electronic Eigen value $\varepsilon_n(R)$ depends parametrically on nuclear position. It will give rise to a surface called *Born-Oppenheimer surface.*

2.4 **Electron-Electron Interaction:**

The election-electron Coulomb interaction, is long-ranged and, for short distances, very strong on and is a big challenge in theoretical study of solid state physics. $V_{e\text{-}e}$ since it is a two-body interaction embedded in a many-body problem, the equation is still a partial differential equation with 3N coupled degrees of freedom which cannot be solved exactly. Out of many methods to take care of this interaction, we describe effective field approximation or, 'effective one particle theory'.

2.4.1 Hartree Approximation:

Hartree proposed that the total electron wave function can be written as a product of individual one-electron orbitals. Furthermore, each electron moves in an "effective" external field, known as Hartree Self-Consistent Field (HSCF)[5-6], created by all other electrons and ions in the background. The Hartree form Schrödinger equation for the i^{th} electron can be derived to be:

$$\left[-\frac{\hbar^2}{2m}\nabla_i^2 + \sum_I V(R_I, r_i) + \sum_{j\neq i}\int \frac{\left|\Phi_j(r_j)\right|^2}{\left|r_j - r_i\right|} dr_j\right]\Phi_i(r_i) = \varepsilon_i\Phi_i(r_i) \quad (2.4.12)$$

Where the potential terns are collectively called effective potential $v_{eff}(r) = v_{ext}(r) + v_{Hartree}(r)$, and $\left|\Phi_j(r_j)\right|^2 = \rho(r)$ is the electron density in the background.

By applying the variational principle that the 'n' one electron orbitals construct the ground state of the system, we can find the HSCF energy to be

$$E_{HSCF} = \sum_{i=1}^{N} \varepsilon_i - \frac{1}{2}\sum_{i \neq j}^{N} J_{ij} \qquad (2.4.13)$$

Here the first term is the sum of the Eigen values of the one electron orbital states, seconds term is the sum of the energies of each electron state in the electron cloud of the rest. This equation is again 'N' coupled differential equation and the potential depends on the wave function, the equation is solved iteratively. Note the constant factors are dropped in Hartree units.

Even though it is a great achievement, Hartree formalism is not applicable and not accurate at all, as it takes electrons as distinguishable particles which actually are not. The problem lies in the definition of the wave function, which does not follow Pauli's principle of occupation.

2.4.2 Hartree - Fock Approximation

It is an extension of the HA based on Slater's work[7-9]. It takes the wave function to be not the simple product but the Slater determinant of the individual electrons. It thus takes care of the Pauli Exclusion Principle making sure that that the total wave function for the fermionic system is antisymmetric under exchange of any two electrons. As includes the permutation symmetry of the wave function, leads to the exchange that is the energy functional includes an extra exchange term than the Hartree energy functional. The equation of based on the approximation can be derived as

$$\left[-\frac{\hbar^2}{2m}\nabla_i^2 + \sum_I V(R_I, r_i)\right]\Phi_\lambda(r_i)$$

$$+\left[\sum_\mu \int \phi_\mu^*(r_j)\frac{1}{|r_i - r_j|}\phi_\mu(r_j)dr_j\right]\Phi_\lambda(r_i) \qquad (2.4.14)$$

$$-\sum_\mu \left[\int \phi_\mu^*(r_j)\frac{1}{|r_i - r_j|}\phi_\lambda(r_j)dr_j\right]\Phi_\mu(r_i)$$

$$= \varepsilon_i \Phi_\lambda(r_i)$$

The last term in LHS describes the exchange effect of two fermions. Since the exchange term has a negative sign, it will reduce the Hartree energy which is as follows:

$$E_{HF} = \sum_{i=1}^{N} \varepsilon_i - \frac{1}{2}\sum_{i\neq j}^{N}(J_{ij} - K_{ij}) \qquad (2.4.15)$$

Here, K_{ij} represents the exchange integrals. HF, therefore, is a better than the Hartree approximation. Hartree and Hartree-Fock formalism point out that electrons with the same spin do not move independently from one another but are correlated. HF accounts for most of the total energy, but, as the Coulomb potential is considered on a mean field level that does not count the correlation effects - actual electron-electron pair interaction.

2.5 **Density Functional Theory**

At the same time, Hartree developed his approximation, Thomas-Fermi was working independently to solve the issues. He assumed the charge density as the fundamental variable of the many body problem and the energy can be expressed through the electron

density. It is an important theory since it is regarded as an approximation to the exact theory: the Density Functional Theory.

By its name, density Functional Theory [DFT], is a theory based on the charge density. This is one of the most powerful tools of understanding ground state electronic structure of the material.

The quantum mechanical theory has come up in the form from the contribution of Hohenberg and Kohn (1964) and Kohn and Sham (1965) describing the effects of exchange and correlation in an electron gas and followed by number of approximations.

2.5.1 Hohenberg-Kohn (HK) Theorem:

H-K formulated and proved a theorem that put mathematical grounds for the T-F theorem. It runs over two statements[10-11]:

1st statement: the ground state electronic density uniquely determines the external potential with some additive constant. More explicitly, if two systems of electrons experiencing two different potentials $V_1(r)$ and $V_2(r)$ respectively both having the same ground state electronic density $\rho(r)$, then $V_1(r) - V_2(r) = const.$ Thus, rather remarkably, a knowledge of $\rho(r)$uniquely determines the entire Hamiltonian operator and the total energy including the exchange and correlation.

2nd statement: for a given external potential v ($\boldsymbol{r}$), and there exists a functional of electron density $\rho(r)$defined as

$$E[\rho] = F[\rho] + \int v(r)\, \rho(r) dr \qquad (2.5.16)$$

Where$F[\rho]$ is a functional of electron density defined, with extension given by Levy and Lieb as

$$F[\rho(r)] = \min(\psi(T+U)\psi) \qquad (2.5.17)$$

where the ψ s range over all antisymmetric n-particle wave functions giving rise to the density $\rho(r)$and U is e-e interaction energy.

By using the conventional Rayleigh-Ritz variational principle it is proved that functional $E[\rho]$attains its minimum value when $\rho(r)$ is the ground state density, and that its minimum value is the ground state energy. $F[\rho]$ is remarkable as the universal functional only of the density. H-K conclude that the electron density determines all the properties of ground state of a system of multi-electrons, however, do not provide the insight as to how to obtain it.

2.5.2 Kohn-Sham Equation:

It is one of the most powerful equation in solving many body problems that includes the exchange and correlation effects. It is based on the statements[10, 12] that

1. Non-interacting systems of electrons will be described by antisymmetric wave function as given by Slater's determinant.
2. The potential of non-interacting systems, called reference potential, yields the density of real interacting system.
3. The ground state energy of the interacting system coincides with that of the non-interacting system.

The wave function of the non-interacting system of electrons is

$$\phi(r) = \frac{1}{N_s}\begin{vmatrix} \phi_1(r_1) & \phi_1(r_2) & \dots & \dots \\ \phi_2(r_1) & \phi_2(r_2) & \dots & \dots \\ \dots & \dots & \dots & \dots \\ \dots & \dots & \dots & \phi_{N_s}(r_{N_s}) \end{vmatrix} \quad (2.5.18)$$

And ground state charge density is

$$\rho(r) = \sum_{i=1}^{N} f_i \, \phi_i(r)\phi_i^*(r) \quad (2.5.19)$$

Where ϕ_i are the electronic orbital and f_i are corresponding occupation number.

The Hamiltonian of the non-integrating system is

$$\hat{H} = \sum_{i=1}^{N}\left[-\frac{\nabla_i^2}{2} + V_R(r_i)\right] \quad (2.5.20)$$

Where N is the number of electron and V_R is the potential of the non-interacting system called reference potential.

Now, for the 2-electron potential system, $N_s = \frac{N}{2}$ and $f_i = 2$ for $N_s \leq \frac{N}{2}$ and $f_i = 0$ for $N_s < \frac{N}{2}$ and the ground state charge density would be

$$\rho(r) = 2\sum_{i}^{N}\left|\phi_i(r)\right|^2 \quad (2.5.21)$$

Here ϕ_i resembles the one electron orbital, the fictitious quasi particle orbital whose sum of the norm coincides with the ground state charge density of the real e-e interacting system. These quasi orbitals, called Kohn-Sham's orbitals, are the solution of the Eigenvalue equation

$$H_{K-S}\phi_i = \varepsilon_i\phi_i \quad (2.5.22)$$

where H_{K-S} is one particle Hamiltonian

$$H_{K-S} = -\frac{\nabla_i^2}{2} + V_R(r_i) \tag{2.5.23}$$

Thus, the problem of many particle system is reduced to one particle problem no matter how many particles are contained in the system[13]. These equations are called Kohn-Sham equation.

2.5.3 Reference Potential:

The kinetic energy of fully integrated system is

$$T_R[\rho] = -\frac{1}{2}\sum_{i=1}^{N_s}\langle\phi_i|\nabla^2|\phi_i\rangle \tag{2.5.24}$$

And the universal functional $F[\rho]$ takes the form

$$F[\rho] = T_R[\rho] + \frac{1}{2}\int \frac{\rho(r)\rho(r')}{|r-r'|}dr\,dr' + E_{xc}[\rho] \tag{2.5.25}$$

Plugging $F[\rho]$ into

$$E[\rho] = F[\rho] + \int \rho(r)v_{ext}(r)dr \tag{2.5.26}$$

We get,

$$E_{KS}[\rho] = T_R[\rho] + \int \rho(r)v_{ext}(r)dr + \frac{1}{2}\int \frac{\rho(r)\rho(r')}{|r-r'|}drdr' + E_{xc}[\rho] \tag{2.5.27}$$

Using Lagrange Multiplayer and constraint $\int \rho(r)dr = N$, we get,

$$\frac{\delta}{\delta\rho(r)}\left\{E_{KS}[\rho] - \mu\left(\int \rho(r)dr - N\right)\right\} = 0 \tag{2.5.28}$$

$$\mu = \frac{\delta T_R[\rho]}{\delta\rho(r)} + v_{ext}(r) + \int \frac{\rho(r')}{|r-r'|}dr' + \frac{\delta E_{xc}[\rho]}{\delta\rho(r)} \tag{2.5.29}$$

The energy for the non-interacting system is

$$E_R[\rho] = T_R[\rho] + \int \rho(r) v_R(r) dr \tag{2.5.30}$$

Similarly,

$$\frac{\delta}{\delta\rho(r)}\left\{E_R[\rho] - \mu_R\left(\int \rho(r)dr - N\right)\right\} = 0 \tag{2.5.31}$$

$$\Longrightarrow \qquad \mu_R = \frac{\delta T_R[\rho]}{\delta\rho(r)} + v_R(r) \tag{2.5.32}$$

Since the energy of the non-interacting system should be equal to the energy of the interacting one at ground state, and the number of particles is the same in the system, the chemical potentials μ and μ_R should be equal,

$$V_R(r) = v_{ext}(r) + \int \frac{\rho(r')}{|r-r'|}dr' + \frac{\delta E_{XC}[\rho(r)]}{\delta\rho(r)} \tag{2.5.33}$$

This is also called effective potential $V_{eff}(r)$.

The Kohn-Sham equation takes the form:

$$\left[-\frac{1}{2}\nabla^2 + V_{eff}(r) - \varepsilon_i\right]\phi_i(r) = 0 \tag{2.5.34}$$

It is important to note that the potential is the functional of charge density which is function of the Kohn-Sham orbitals. So the Kohn-Sham equation is solved self consistently.

Total energy:

By inserting the$v_{ext}(r)$, we get the total energy of the interacting system as

$$E_{KS}[\rho] = T_R[\rho] + \int \rho(r) v_{eff}(r) dr - \frac{1}{2}\int \frac{\rho(r)\rho(r')}{|r-r'|} dr dr' + E_{xc}[\rho] - \int \rho(r) \frac{\delta E_{XC}[\rho(r)]}{\delta \rho(r)} dr \tag{2.5.35}$$

First two terms represent the energy of the non-interacting system, i.e.

$$E_R[\rho] = T_R[\rho] + V_R(r) \tag{2.5.36}$$

$$= \sum_i \left\langle \phi_i \middle| -\frac{\nabla^2}{2} \middle| \phi_i \right\rangle + \int \rho(r) v_{eff}(r) dr$$

$$= \sum_i \int \phi_i^* \left(-\frac{\nabla^2}{2} + v_{eff}(r) \right) \phi_i \, dr$$

$$\Longrightarrow \qquad E_R[\rho] = 2 \sum_i^{N/2} \varepsilon_i \tag{2.5.37}$$

i.e. the sum of the single electron Eigenvalues. Factor 2 comes from the spin degeneracy. Thus the total energy of the Kohn-Sham system is given by

$$E_{KS}[\rho] = 2 \sum_i^{N/2} \varepsilon_i - \frac{1}{2}\int \frac{\rho(r)\rho(r')}{|r-r'|} dr dr' + E_{xc}[\rho] - \int \rho(r) \frac{\delta E_{XC}[\rho(r)]}{\delta \rho(r)} dr \tag{2.5.38}$$

First two terms in this equation are known. With this progress, the problem of determining the minimization of the H-K universal functional has been transformed to the single term $E_{xc}[\rho(r)]$. So. The challenge remains to finding the exact form of it.

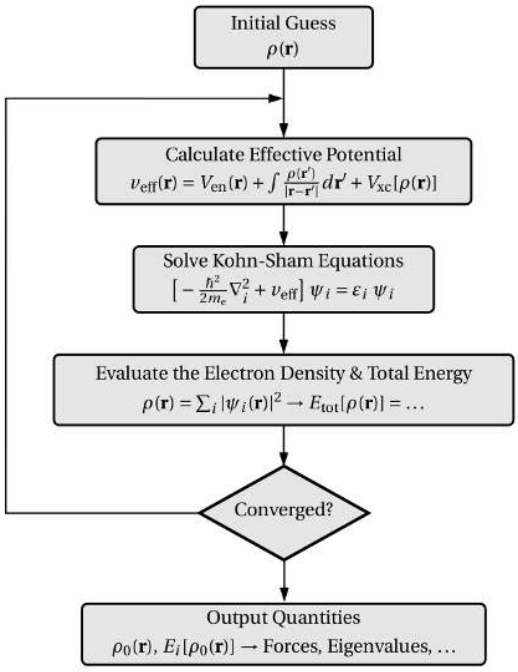

Figure 2: A flow chart of the self-consistent iteration scheme:.

The self-consistent iteration process of solving the KS equation is shown in in fig. 2 The Initial assumed electron density is used for the calculation of $v_{eff}(r)$, the diagonalization of the Kohn-Sham equations, and the subsequent evaluation of ρ(r) along with $E_{tot.}$ At that point it is checked whether the calculation is converged or not. If not, it is continued again with the last $\rho(r)$ as the new density. After the system is converged, various output quantities to be studied are computed

2.5.4 Approximation for $E_{xc}[\rho(r)]$:

W. Kohn devised the most important approximation for $E_{xc}[\rho(r)]$ as having a quasilocal form that can be written as

$$E_{xc}[\rho(r)] = \int \varepsilon_{xc}(r, [\rho(\tilde{r})])\rho(r)dr \tag{2.5.39}$$

Where $\varepsilon_{xc}(r, [\rho(\tilde{r})])$ is an exchange correlation energy per particle at a point r which is a functional of density $\rho(\tilde{r})$ at $\tilde{r}$ near r. The microscopic distance between the two points is such that the fermi wavelength is

$$\lambda_F(r) = [3\pi^2\,\rho(r)]^{-\frac{1}{3}} \tag{2.5.40}$$

2.5.4.1 Local Density Approximation [LDA]:

This simplest approximation assumes the density of elections to be uniform i.e.

$$E_{xc}^{LDA} = \int \varepsilon_{xc}(r, [\rho(r)])\rho(r)dr \tag{2.5.41}$$

Here the exchange correlation energy per particle $\varepsilon_{xc}([\rho(r)])$ is functional of the charge density $\rho(r)$.

Than exchange part of the energy is given by

$$\varepsilon_x = -\frac{0.458}{r_s} \tag{2.5.42}$$

Where, r_s is the radius of the sphere containing one electron which is given as

$$\frac{1}{\rho} = \frac{4\pi}{3} r_s^3 \tag{2.5.43}$$

This is an exact solution for the uniform electronic gas. And correlation part cannot be calculated exactly even for the uniform electronic gas. One simple approximate solution [E.P Wigner 1938][14] is

$$\varepsilon_c = \frac{0.44}{r_s + 7.8} \tag{2.5.44}$$

High precise value is suggested more recently by Ceperley and Alder [1980][15] using Monte Carlo method.

LDA is exact for the uniform electron gas, however in atomic systems these conditions are hardly satisfied. Also, LDA badly overestimates (up to ~ 20%) cohesive energies and bond strengths in molecules and solids, and as a consequence bond lengths are often underestimated[16]. Improved approximation is needed to deal with the non-uniform electron density.

Better approximation could be a gradient expansion for E_{xc}. It is based on the expansion of the charge density $\rho(\tilde{r})$ around the point r which we can take to be the origin:

$$\rho(\tilde{r}) = \rho + \rho_i \tilde{r}_i + \frac{1}{2}\sum \rho_{ij}\tilde{r}_i\tilde{r}_j + \cdots. \tag{2.5.45}$$

With

$$\rho = \rho(0), \rho_i = \nabla_i \rho(r)|_{r=0,}\, etc. \tag{2.5.46}$$

Consequently, we get the resultant sequence as

$$E_{XC} = \int \rho(r)\varepsilon_x^{hom}(\rho) F_{XC}(\rho, \nabla\rho, \nabla^2\rho, \ldots\ldots) dr \tag{2.5.47}$$

Where, F_{XC} is a dimensionless quantity called enhancement factor.

This is still semi-local approach and long range effects are not taken into account. The expansion is not stable as it does not converge monotonically and has singularities that are eliminated only when an infinite number of terms are taken into account.

Approximation is required that mimics the summation to infinite order and assures the condition of long range decay. Different authors tried to fix the problem, one of the most successful approximations is Generalized Gradient Approximation.

2.5.4.2 Generalized Gradient Approximation [GGA].

It is an advancement of the LDA and brings up the contribution of the energy that is the functional of differential form of the charge density:

$$E_{XC} = \int \rho(r)\varepsilon_x^{hom}(\rho)F_{XC}(\rho, \nabla\rho)dr \tag{2.5.48}$$

Several GGAs have been in practice. Each of them purpose different form of the enhancement factor. One of the most widely used is one purposed by Perdew, Burke and Ernzerhof (PBE)[17]. In this approximation the enhancement factor corresponding to the exchange contribution is given as,

$$F_x(s) = 1 + k - \frac{k}{1 + \frac{\mu s^2}{k}} \tag{2.5.49}$$

where, $\mu = 0.21951, k = 0.0804$ and $s = \frac{|\nabla\rho(r)|}{2k_F\,\rho}$

And, the correlation contribution to the energy is given as:

$$E_C^{GGA} = \int \rho(r)[\varepsilon_c^{LDA}(\rho, \xi) + H(\rho, \xi, t)]dr \tag{2.5.50}$$

Where, $H(\rho, \xi, t)]$ is a function of charge densityρ, magnetization ξ, while t is also a function of $\rho\ and\ \xi$ that can be found in literature[11].

2.6 Periodic System: Super cell Approximation

As shown in preceding section, many body problem can be mapped into an effective single particle problem. However, for a macroscopic system the problem still persists in dealing with 10^{23} -10^{25} non-interacting electrons moving in the static potential

of 10^{22} -10^{23} ions. Two difficulties arise in front: a wave function must be calculated for each of the electron in the system, and, since each electron wave function extends over the entire solid, the basis set required to expand each wave function is infinite in a microscopic terms. Both problems can be addressed by performing calculations on periodic systems and apply the Bloch's theorem to the electronic wave functions.

2.6.1 Bloch Theorem

Bloch's theorem states that in a periodic solid each electronic wave function can be written as the product of a cell-periodic part and a wavelike part[18],

$$\psi_i(r) = \exp[\mathrm{ik.r}] f_i(r) \tag{2.6.51}$$

The cell periodic part of wave function, $f_i(r)$, that reduces a problem of infinite crystal to the problem of one unit cell. It can be expanded using a basis set consisting of a discrete set of plane waves whose wave vectors are reciprocal lattice vectors of the crystal,

$$f_i(r) = \sum_G c_{i,G} \exp[iG.r] \tag{2.6.52}$$

Where the reciprocal lattice vector G are defined by $G.l = 2\pi m$ for all l where l is a lattice vector of the crystal and m is an integer. Hence each electronic wave function can be written as the sum of the plane wave;

$$\psi_i(r) = \sum_G c_{i,k+G} \exp[i(k+G).r] \tag{2.6.53}$$

2.6.2 K-point Sampling

Electronic states are allowed only at a set of k points determined by the boundary conditions that apply to the bulk solid. The density of allowed k points is proportional to the volume of the solid. The infinite number of electrons in the solid are accounted for by an infinite number of k points, and only a finite number of electronic states are occupied at each k point. Consequently, it is possible to represent the electronic wave functions over a region of k space by wave function at a single k point and the electronic states calculated at only finite number of k points will provide the total energy of the system.

The calculation of the contribution to the total energy from the filled electronic band is determined by calculating the electronic states at special sets of k points in Brillouin zone[19]. Basically, the calculation is done over k points in the region of the irreducible BZ.

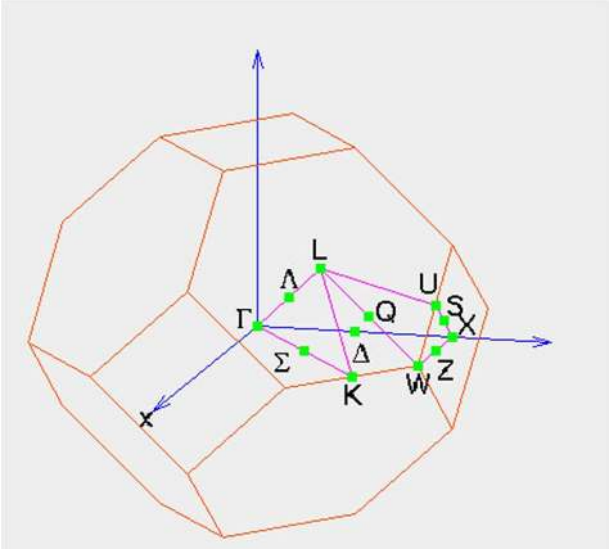

Figure 3: IBZ for the FCC lattice (pink lines). Each symmetric point or direction has a special notation

2.6.3 Plane Wave Basis Sets

According to the Bloch's theorem the electronic wave functions at each k point can be expanded in terms of a discrete plane-wave basis set. In principle, an infinite plane-wave basis set is required to expand the electronic wave functions. However, the coefficients $c_{i,k+G}$ for the plane waves with small kinetic energy $\frac{1}{2}|k+G|^2$ are typically more important than those with large kinetic energy. Thus the plane-wave basis set can be truncated to include only plane waves that have kinetic energies less than some particular cutoff energy. Introduction of an energy cutoff to the discrete plane-wave basis set produces a finite basis set. The number of plane waves and hence the cutoff energy depends of the Hamiltonian matrix of the system; and will be incredibly very large for systems that contain both valence and core electrons. This severe problem can be overcome by the use of pseudopotential approximation.

2.6.4 Pseudopotential Approximation

Although Bloch's theorem allows the electronic wave functions to be expanded using a discrete set of plane waves, a plane-wave basis set is usually very poorly suited to expanding electronic wave functions because a very large number of plane waves are needed to expand the tightly bound core orbitals and to follow the rapid oscillations of the wave functions of the valence electrons in the core region. An extremely large plane-wave basis set would be required to perform an all-electron calculation, and a vast amount of computational time would be required to calculate the electronic wave functions. The pseudopotential approximation (Phillips, 1958[20]; Heine and Cohen, 1970[21]; Yin and

Cohen, 1982[22]) allows the electronic wave functions to be expanded using a much smaller number of plane-wave basis states.

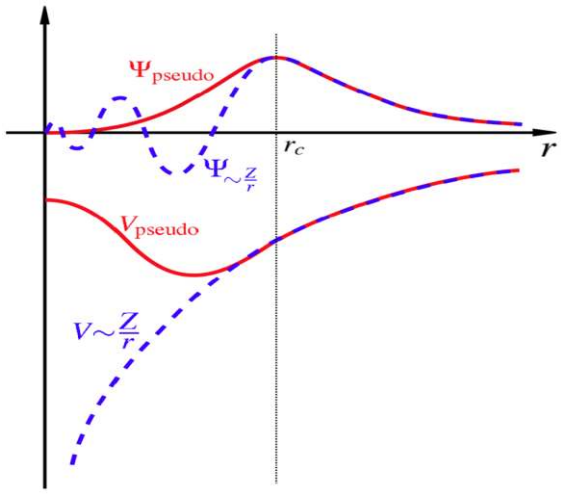

Figure 4: Schematic illustration of all-electron (dashed lines) and pseudo electron (solid lines) potentials and their corresponding wave functions. The radius at which all-electron and pseudo electron values match is designed r_c.

As shown in the figure. 4, the, the potential is designed in such a way that the fast oscillating wave function near the core is made smooth and symmetric about the point r_c.

2.7 Techniques of Solving Kohn-Sham Equation

2.7.1 VASP:

VASP is a complex multifunctional software package that performs ab-initio quantum-mechanical simulations using pseudopotentials and plane wave basis set. The calculations performed using this code provide valuable information on various physical and chemical properties of material systems. In these projects we performed calculations of total energy of the systems, densities of electronic states, electronic charge densities and

vibrational frequencies of various components of the systems of interest. All these quantities are defined for the electronic ground states and thus can be obtained within DFT. Here are some of important features of the VASP code:

a) Since VASP uses the PAW method or ultra-soft pseudopotentials, the size of the basis-set can be kept very small even for transition metals and first row elements like C and O.

b) As in any plane wave program, the execution time scales like N^3, N the number of valence electrons, in VASP, but the pre-factors for the cubic parts are almost negligible leading to an efficient scaling with respect to system size.

c) The full featured symmetry code included in VASP determines the symmetry of arbitrary configurations automatically and is used to set up the Monkhorst Pack special points allowing an efficient calculation of bulk materials, symmetric clusters.

d) VASP runs equally well on super-scalar processors, vector computers and parallel computers.

2.7.2 Density of States:

It is one of the primary quantities used to describe the electronic state of a material. It measures how the quantum states that the electrons can stay in. It is defined as the number of electron states with energy in interval $(E, E + dE)$ and denoted by N(E) . In DFT calculation electronic DOS is calculated by integrating the resulting electronic density in k-space. DOS is one of an important handy tools to study electronic properties of the

material[23]. The reactivity of a material is defined in part based on how the DOS is distributed about the fermi level[24].

2.7.3 Charge Distribution: Bader Analysis

As we've seen that almost all reactions or bond formations are possible by charge transfer between the partner atoms. Again, atomic charges in molecules or solids are not well-defined. The output of DFT calculation is continuous electronic charge density and it is not clear how one should partition electrons amongst fragments of the system such as atoms or molecules. Many different schemes have been purposed, some are based on electronic orbitals (Mulliken Population Orbitals, Density matrix based normal population analysis.) and others are based on charge density (Bader analysis and Hirshfeld analysis[25]). The Bader Analysis is found to be the most convincing.

2.7.3.1 Bader Analysis:

It is a tool to calculate the charge on individual atoms in Molecule and crystal. Richard Bader developed an intuitive way of dividing molecules into atoms called the Quantum Theory of Atoms in Molecules (QTAIM)[26]. His definition of an atom is based purely on the electronic charge density. Bader uses what are called zero flux surfaces to divide atoms. A zero-flux surface is a 2-D surface on which the charge density is a minimum perpendicular to the surface[25, 27]. Typically in molecular systems, the charge density reaches a minimum between atoms and this is a natural place to separate atoms from each other. Bader's theory of atoms in molecules is often useful for charge analysis. For example, the charge enclosed within the Bader volume is a good approximation to the

total electronic charge of an atom. The charge distribution can be used to determine multipole moments of interacting atoms or molecules. Bader's analysis has also been used to define the hardness of atoms, which can be used to quantify the cost of removing charge from an atom. The theory also provides a definition for chemical bonding that gives numerical values for bond strength.

Henkelman's group[25] has developed computational method for partitioning a charge density grid into Bader volumes which is efficient, robust, and scales linearly with the number of grid points. The partitioning algorithm follows steepest ascent paths along the charge density gradient from grid point to grid point until a charge density maximum is reached. As the algorithm assigns grid points to charge density maxima, subsequent paths are terminated when they reach previously assigned grid points. It is this grid based approach which gives the algorithm its efficiency, and allows for the analysis of the large grids generated from plane wave based density functional theory calculations.

2.7.4 Electrochemical Reaction and Fuel Cell:

Chemical reaction carried out by the actual transfer of proton or other charged species (ions) is electrochemical reaction, it ultimately gives out some potential difference that drives current in the external circuit.

2.7.4.1 Mechanism of Reaction in Hydrogen Fuel Cell:

The Hydrogen gas molecule going over anode gets dissociated into atoms and adsorbed on the anode surface. The hydrogen atom is oxidized giving out electron and the hydrogen ion(H^+). The H^+ passes through the PEM to cathode while the electron is set

free to move through the external circuit constituting current. At the cathode, the oxygen gets reduced taking electron from the circuit and combines with the H^+ giving rise to water molecule. The overall reaction is summarized below:

At anode:

$$H_2 \rightarrow 2H^+ + 2e^- \tag{2.7.54}$$

At cathode:

$$\frac{1}{2}O_2 + 2H^+ + 2e^- \rightarrow H_2O \tag{2.7.55}$$

Overall reaction:

$$H_2 + \frac{1}{2}O_2 \rightarrow H_2O \tag{2.7.56}$$

To obtain an appropriate reaction rate it has to be promoted by the catalysts. Not a single catalyst is found yet that works perfect. The Platinum is found to be most effective for both anode and cathode reactions, however, it has many shortcoming. So, much attention is drawn to seek the suitable electrocatalysts to carry on the reactions effectively so that the performance of the fuel cell is optimized.

2.7.4.2 Reaction rate and Catalytic action.

Electrochemical behavior is evaluated by reaction rate. The speed of reaction determines its effectiveness. The rate of reaction depends on the electronic properties of the material that promotes the reaction, the electrocatalyst. In some cases, we have to promote the reaction rate while some cases are there where we have to suppress the speed of reaction. From the knowledge of the rate of a particular reaction with a particular

catalyst, we can optimize it by modeling the suitable combination of catalysts with different catalytic activities.

Schematically, the action of catalyst can be studied in the following way: Chemical reactions proceed from the collision of the reacting molecules. There is a great impact of the temperature as the collision is promoted by the rise of temperature. Arhinues theorem provides the impact of the temperature on the rate of reaction as

$$R = Ae^{-\frac{E_a}{K_B T}} \tag{2.7.57}$$

Where A is the frequency factor that depends on the rate at which the reaction goes forward and backward, more explicitly the number of times the molecules collide[28-29], E_a is the activation energy that basically determines the barrier to the reaction path and others have usual meaning. Often, the pre-exponential factor A and activation energy E_a are temperature dependent. The activation energy is involved in breaking the bond of the molecules and let form the new bonds in new structures about the boundary called the transition state.

The collision theory, which assumes that the two atoms with certain amount of activation energy, collide to react, gives the expression for the frequency factor modifies the Arhinues equation as

$$R = \pi\sigma^2 N \left(\frac{8K_B T}{\pi\mu}\right)^{\frac{1}{2}} e^{-\frac{E_a}{K_B T}} \tag{2.7.58}$$

Where, σ is sum of the diameters of two atoms, μ is the reduced mass of the two atoms. Transition state Theory, which was developed simultaneously by Henry Eyring, Meredith Gwynne Evans and Michael Polanyl, assumes a quasi-equilibrium state between the

reactants and the products of the reaction. Based on the quantum mechanical calculation, by introducing the entropy of activation, they introduced the Gibb's Free Energy of activation instead of the activation energy. The reaction rate takes the form as

$$R = \frac{K_B T}{\hbar} e^{-\frac{\Delta G}{K_B T}} \tag{2.7.59}$$

Where

$$\Delta G = \Delta E - \Delta ZPE - T\Delta S \tag{2.7.60}$$

Where, E is the total energy of the system, ZPE is the zero-point energy and S is the entropy.

2.7.4.3 Action of Catalyst:

A catalyst increases the rate of a reaction by providing a reaction path with a low activation energy. Action of the catalyst can be explained based of the following schematic energy profile:

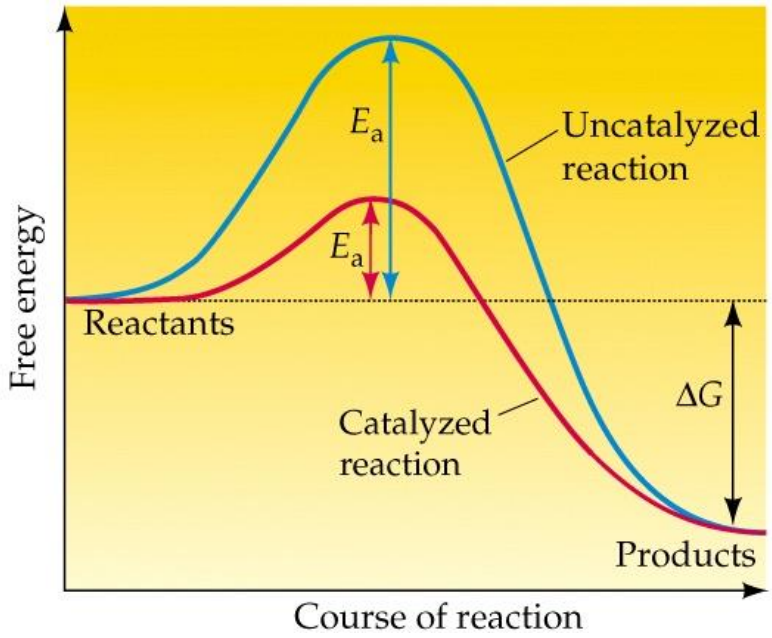

Figure 5: **Action of catalyst. Catalyst lowers the activation energy of the reaction.**

2.8 **Conclusion**

The problem of many body system is solved by using a sophisticated well stablished mathematical model 'Density Functional Theory'. It runs over the recipe of solving the Kohn-Sham equation with all the input parameters and supporting quantities supplied for the particular situation. VASP 5.3 is used to calculate the quantities that we look for describing the electrocatalytic properties of the material systems we considered.

CHAPTER 3
Pd/W(110) AS A HIGHLY CO TOLERANT ELECTROCATALYST FOR HYDROGEN OXIDATION: INSITE FROM FIRST PRINCIPLES

3.1 **Introduction**

The proton exchange membrane fuel cells (PEMFC) are a very promising means for clean conversion of chemical energy stored in hydrogen into electric energy. However, there are several obstacles hindering their large-scale applications. In PEMFC, hydrogen is oxidized to H^+ on anode. Then protons are transferred through a solid electrolyte membrane to cathode where oxygen reduction reaction (ORR) takes place. One obstacle is that both reactions, hydrogen oxidation reaction (HOR) and ORR, are currently facilitated by electrocatalysts, which contain a significant amount of very expensive and scarce Pt and/or other Pt-group elements (PGE). It is thus not surprising that a great effort has been made to replace (at least partially) these elements with cost-effective materials.

The other problem is that activity of these catalysts is still not as high as desired. In fact, Pt has a very high activity toward HOR[30], but this is the case only if one deals with pure hydrogen. However, currently most of hydrogen is produced from hydrocarbons and the corresponding reactions have CO among the products. Available procedures of purification of hydrogen are not quite efficient in terms of CO removal[31]. If CO comes together with H_2 to Pt anode of PEMFC, it strongly binds to Pt surface sites making them not available for HOR, which is known as CO poisoning of the catalyst. Unfortunately, even small traces of CO poison Pt severely[32]. In this chapter we summarize the works done and attempts made to solve the problem and come up with an idea that has been seen so promising in dealing with this issue.

3.2 Review of the past works and our effort

A significant progress has been made in solving this problem. It has been found that PtRu alloys are more tolerant to CO poisoning than Pt[33-34]. The Ru sites in the alloy are very reactive and water present in the reaction environment dissociates on the Ru sites leaving OH adsorbed. Next, OH reacts with CO adsorbed in neighboring Pt sites producing CO_2 that easily desorbs from the catalyst. This is known as bi-functional reaction mechanism[35]. In addition, hybridization between Pt- and Ru-d-electronic states reduces reactivity of Pt sites that also eases CO removal[35-36]. The RuPt alloys are currently widely used as anodic catalysts for PEMFC. The Pt alloys with several other metals have also been tested as the HOR catalysts[37-39]. Although some alloys, are more tolerant to CO poisoning than Pt and even than PtRu, their main disadvantage is that they still contain a large fraction of Pt. A significant reduction of Pt load has been reported in Refs[40-41]. In that work, a sub-monolayer of Pt was deposited on ~2.5 nm Ru nanoparticles with Pt/Ru content ratio 1/20. These systems, in addition to low Pt content, appeared to be much more tolerant to CO poisoning than PtRu alloys. Results of first principles calculations suggested that small Pt islands formed on Ru facets[42] have a potential energy profile that leads to spillover of CO molecules from islands, and, as CO reaches the island edge, it readily reacts with available OH to form CO_2[43]. Nanoparticles with well-defined bilayer Pt shell on the single Ru core Ru@Pt, resolve the dilemma in using a dissolution-prone metal for alleviating the deactivating effect of CO Ref.[44]. Ordered structural transition from Ru (hcp) to Pt (fcc) stacking brings about some shifting the position of Ru at the interface as the partial alloy prefers fcc structure. These nanostructures have a great advantage over PtRu alloys in terms

of both Pt load 25μgcm^{-2} (Ru@Pt) whereas 50-100μgcm^{-2} (Ru-Pt alloy) and CO tolerance. Detailed DFT studies of Ru@Pt, Ir@Pt, Rh@Pt, Pd@Pt and Au@Pt core shell structures versus Pt suggested that Ru@Pt is the only structure with remarkably lower CO saturation coverage compared with the pure Pt[45]. However, their main component Ru is still prohibitively expensive for large-scale applications. In addition, electrochemical stability of Ru is unsatisfactory for PEMFC application[46].

Pt-W alloys, with composition ranging from Pt_3W to PtW_2, possess superior CO tolerance to Pt and PtRu[47], mainly due to the weakened bonding of CO on their Pt-enriched surfaces. It is shown that it leads to enhanced electrocatalytic activity for HOR, with nearly 4 times increase in the exchange current density as compared with pure Pt.

Pt nanoparticle supported on $Ti_{0.7}W_{0.3}O_2$ exhibited a unique CO-tolerant electrocatalytic activity as it operates large decrease in overpotential and lowest onset potential the for H_2 oxidation (ca. 0.05 V vs RHE) relative to both Pt/C and PtRu/C[48].

A reasonable direction for further reduction of cost of the HOR catalysts is to explore structure with an active element (Pt or others) deposited on substrates not containing PGE. There are several works heading alone this direction. For example, authors of Ref.[49] deposited Pd, PdRu, PdIr nanoparticles on WO_x and studied their tolerance to CO poisoning during HOR. They found it to be better than that of Pt, but not as good as that of the PtRu alloys. The authors do not discuss stability of this system. However, a similar structure – small Pt nanoparticles on WO_x substrate has been reported as unstable[50]. Furthermore, there are many studies[51-54] on this structure and authors explain about the activities of the catalyst without mentioning the stability.

Authors of Ref.[55] have discussed on the CO tolerance of molybdenum carbide-based electrocatalysts. It is shown that the catalyst Mo_2C/C is in one hand more stable than PtMo/C and Pt/C catalyst; one the other hand, more effective for the CO oxidation especially at high temperature. For the $Pt/Mo_2C/C$, $PtMo/Mo_2C/C$ and PtMo/C catalysts, part of CO is adsorbed on Pt surface and part is directly oxidized to CO_2 whereas for Pt/c catalyst, the only process is the adsorption on the catalyst surface.

Ref. [56] has reported that the carbon supported Pd-Au alloy nanoparticles exhibit an outstanding CO tolerance during HOR at low overpotentials. The alternation of electrocatalytic and adsorption properties of palladium under the action of gold substrate is brought about by the modification of d-band center of the Pd caused by a strain of the Pd lattice[57] from the interaction with substrate. Besides this electronic effect, the change in chemical composition also brings some changes in catalytic properties called ensemble effect[58-61]. By confirming the possibility of incorporation of carbon into the PdAu alloy and shows substantially enhanced catalytic performance due to promoting action of carbon in PdAu-C_x. is showed enhanced substantially.

We propose an alternative approach that implies deposition of a monolayer of a catalytically active element (AE) on an inexpensive metal substrate (MS). There are several requirements to make this approach successful. First, the proposed system should be thermodynamically stable. The main conditions for that are[62]: a) the lattice mismatch (difference in the interatomic bond length) between AE and MS should be small; b) AE – MS bonds must be stronger than AE – AE bonds. Otherwise AE atoms will prefer to make AE clusters rather than make stable monolayer coverage over the MS substrate; c) the MS

– MS bonds must be stronger than AE – MS bonds to avoid AE/MS alloying. Next, hybridization between AE and MS electronic states should optimize reactivity of the AE monolayers. For the reasons explained in the Section III, we expect that the above stability conditions will be met for AE = Ru, Pd, Au monolayers deposited on MS = W (110). It is not easy to predict the AE – MS hybridization effect on the AE reactivity. Therefore, our choice of AEs is dictated by the fact that reactivity of the elemental (111) surfaces of the selected AEs ranges in order: Au < Pd < Ru. We thus expect that some of the selected AE/W (110) structures will have an optimal reactivity for both HOR and CO oxidation.

In this work, we apply first principles computational methods to evaluate thermodynamic stability, as well as activity toward HOR and CO oxidation of the selected AE/MS structures with a hope to reveal a material that is highly active toward HOR and, at the same time, tolerant to CO oxidation.

3.3 **Theory:**

3.3.1 Electrochemical Reaction in PEMFC:

PEMFC uses up gaseous Oxygen and Hydrogen as the fuel. Overall operation runs over the two different reactions in anode and cathode sides.

At anode, the intake hydrogen undergoes oxidation on the surface of electro-catalyst,

$$H_2 \rightarrow 2H^+ + 2e^- \tag{3.2.61}$$

At cathode, the oxygen gas undergoes reduction on the surface of electro-catalyst again,

$$\frac{1}{2}O_2 + 2H^+ + 2e^- \rightarrow H_2O \tag{3.2.62}$$

Overall reaction is

$$H_2 + \frac{1}{2} O_2 \rightarrow H_2O \tag{3.2.63}$$

The semipermeable electrolyte membrane is designed such a way that only the hydrogen ion can pass through it, while the electrons, hydrogen molecules in anode side and, oxygen, water molecules in cathode side are prohibited to cross it. This is because porosity of the electrolyte is such that hydrogen ion having lower diameter than pores can pass through it while others having larger size are blocked. This ensures avoiding of the short circuit, could be caused by leakage of electrons and gas crossover caused by transmission of hydrogen gas. The potential difference developed between the electrodes makes the electron run in the external circuit constituting the current.

3.3.2 The Thermodynamic Limit for Rate of Reaction:

The rapidness of the chemical reaction depends on the barrier of potential between the reactants and products side of the system. It proceeds forward if the activation energy is higher than the barrier. A catalyst provides an alternate reaction pathway with a lower activation-energy barrier.

Gibb's free energy of a system is defined as

$$G = H - TS \tag{3.2.64}$$

where H is enthalpy of the system, T is the temperature, and S is entropy.

Per transition state theory, the rate constant for an electrochemical reaction is a function of the Gibbs free energy[63]. Therefore, the equation is updated as[43]

$$R = De^{-\frac{\Delta G}{K_B T}} \tag{3.2.65}$$

Where, D is a constant depending on temperature. The change in Gibb's free energy is taken in between two sides of the reaction. Here, we consider only the Potential energy part and neglect the kinetic energy contribution to transition.

3.3.3 Removal of CO from Anode:

One of the challenges of the system of PEMFC is the removal of CO that gets adsorbed on the active sites of the anode catalyst which comes in along with the hydrogen fuel. The reaction in anode proceeds as below[64-65]:

$$H_2O(g) + * + * CO \rightarrow * OH + * CO + H^+ + e^- \tag{3.2.66}$$

$$* OH + * CO + H^+ + e^- \rightarrow CO_2(g) + 2H^+ + 2e^- + 2 * \tag{3.2.67}$$

where the * represents the substrate. In first step water molecule splits up into on OH, a hydrogen ion and an electron. The OH gets adsorbed on the substrate. In the second step of the reaction, CO adsorbed gets oxidized to CO_2 with the liberation of extra hydrogen ion and electron.

To make this reaction favorable one needs to achieve a controversial condition: CO has to bind weakly to the catalyst, whereas the catalyst has to be reactive enough to produce enough OH from water.

3.4 **Methodology**

3.4.1 Computational Details:

Catalytic action takes place on the surface of the system. So, we use the flat surface approximation to describe the catalytic properties of the systems that we consider in our study. The materials under consideration have two basic structure fcc and bcc. The surfaces that have the hexagonal surface arrangement of atoms are considered in both structures. Specifically, we performed calculations of electrocatalytic properties on fcc Pt (111), hcp Ru (0001) and bcc of M/W (110); [M = Pd, Ru, Au].

For all system under consideration, the electronic structure, energetics and equilibrium atomic configurations are obtained using the VASP5.2 code[66] with projector augmented wave potentials and the Perdew-Burke-Ernzerhof (PBE) version of the generalized gradient approximation (GGA) for the exchange and correlation functional[17]. All systems, except for clean Pd, were calculated taking spin polarization into account. To maintain periodicity, we used supercells with a 5-layer slab and vacuum layer of 15 Å between the two slabs of the active substrate.

For all calculations, the supercells had the (2×2) in-plane periodicity. The *k*-point samplings (8 x 6 x 1) for bcc W (110) and (7x7x1) for fcc Pt, Ru and Au in Brillouin zone used in this work provide sufficient accuracy for the characteristics obtained by integration in the reciprocal space. The cutoff energy of 400 eV was used for the plane wave expansion of wave functions. To achieve structural relaxation, a self-consistent electronic structure calculation was followed by calculation of the forces acting on each atom. Based on this

information the atomic positions were optimized to obtain equilibrium geometric structures in which forces acting on atoms do not exceed 0.01 eV/Å.

The formation energy per atom[67] of the atomic layer with n atoms is defined as:

$$E_{Form} = \frac{1}{n}\left(E_{Layer} - E_{clean}\right) \tag{3.3.68}$$

Where $E_{Clean}\ and\ E_{Layer}$ are the total energies of the system with and without Layer formed on the bulk substrate. The change in formation energy per atom then is defined as

$$\Delta E_{Form} = E_f(AE/W) - E_f(AE/AE) \tag{3.3.69}$$

Where AE = Au, Pd and Ru.

3.4.2 Binding Energy:

To characterize strength of bonding of intermediates (Int = CO, OH) on the catalyst surface we used the adsorption energy defined as follows:

$$E_B(Int*) = E_{Tot}\left(\frac{Int}{\text{Slab}}\right) - E_{Tot}(Int) - E_{Tot}(Slab) \tag{3.3.70}$$

where the three E_{Tot} terms denote the total energies per supercell calculated for the CO or OH adsorbed on the surface, isolated CO or OH molecules and clean slab respectively. Given the total energies of stable systems are negative, E_B(Int) is negative, if adsorption of a specie on the slab is favorable.

3.4.3 Gibb's Free Energy:

We calculated the free energy for CO with respect to CO_2, H_2O and H_2 while for OH with respect to H_2O and H_2. The change in Gibbs free energy of the system is obtained as

$$\Delta G(Int) = \Delta E_{Tot} + \Delta ZPE - T\Delta S \tag{3.3.71}$$

To obtain ZPE, we have calculated the vibrational frequencies of the adsorbed CO and OH using the finite-difference method. Since masses of the intermediates are much smaller than those of the substrate, only the adsorbate modes were considered with the frozen slab atoms. Five displacements were used for each direction with the step of 0.02Å. The zero point energies obtained from the vibrational frequencies were used to calculate the ZPE contributions to the reaction free energies.

Entropic contributions to the reaction free energies were calculated taking the room temperature into consideration[68].

Here we have treated $(H^+ + e^-)$ as the $\frac{1}{2}H_2$. It is based the approximation[69] that the total chemical potential of $(H^+ + e^-)$ is equal to the half of that of hydrogen molecule H_2

The geometric structures of clean and adsorbed surfaces shown in this article have been plotted using the XCRYSDEN software[70].

Change in Gibb's free energy of the two steps of the reaction is defined by using the definition above. As the downhill reactions are spontaneous, we did calculation only for the uphill reactions.

The technique of utilizing the definition of binding energy eliminates the contribution of substrate to the total energy. Entropic contributions of adsorbed CO, OH are also very small and so are neglected. Since there is very small variation of the zero-point energy of CO and OH over the different substrates, by taking the average, we can approximate the Gibb's free energy as below:

$$\Delta G[1\text{-}2] = E_B(OH) + 3.185 \qquad (in\ \ eV) \tag{3.3.72}$$

and,

$$\Delta G[2\text{-}3] = -E_B(\ \ OH) - E_B(\ \ CO) - 4.843 \qquad (in\ eV) \tag{3.3.73}$$

It is found that ΔG depends on Binding Energies.

We calculated the binding energy of H, OH and CO adsorbed on different sites of the systems under consideration. We obtained Gibb's free energy for the CO removal reaction steps with the initial state as the reference state.

3.5 **Result:**

3.5.1 Geometric Structure and Stability of Monolayer on the Substrate:

Since the model of our material consists of monolayer of some, fcc and hcp, structures on the bcc substrate W (110), there can be the effect of lattice mismatch and hence comes the issue of stability of the structure. Therefore, it can be explained in terms of the formation energy of the layer on the substrate. We calculated the formation energy of Pd/Pd (111), Ru/Ru (0001), Au/Au (111) and M/W (110) with M = Pd, Au, Ru. In this process, we developed a relaxed slab of 5 layers of Pd, Ru and Au with 20 atoms and then a layer of four atoms of the respective elements was set at the top. Similarly, we developed

the relaxed 5 layered slab of Tungsten W (110) with 20 atoms. We set the monolayer of Pd, Ru and Au with the M atoms on top of the W atoms.

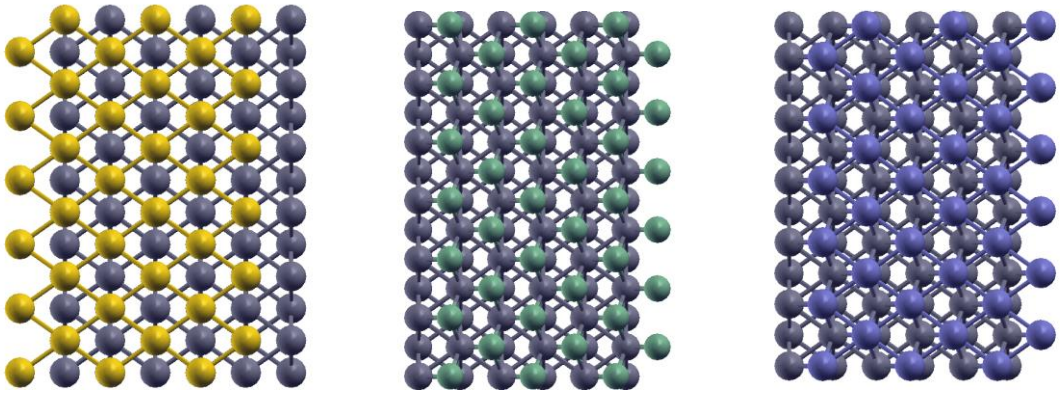

Figure 6: Stable structures of Au(yellowish), Ru(greenish) and Pd(bluish) monolayers on W(blackish) substrate.

Table 1: Difference in formation energy of different structures:

Structure	Pd/W	Au/W	Ru/W
$\Delta E_{form}(eV)$	- 0.849	- 0.532	- 0.216

All the negative values indicate that the formation energy per atom for a monolayer of tungsten on W (110) is higher than that of the active elements. This insures that atoms do not form the island or clusters themselves rather form a stable monolayer on the surface of W (110). Moreover, the binding energy of the tungsten atoms, the cohesive energy, is very high. Consequently, the M-atoms do not penetrate the surface giving rise to the alloy structure.

3.5.2 Adsorption of Hydrogen:

One of the main purposes of the electro-catalyst in PEMFC is to carry out the oxidation hydrogen gas (HOR) in anode. It starts with the dissociation of the H_2 molecule into hydrogen ions (H^+) and electrons (e^-). Possibility of the dissociation of hydrogen molecule on the surface of substrate can be stated observing the dissociative adsorption energy for the structure considered.

Table 2: Atomic Binding Energy and Dissociative Adsorption Energy on the preferred sites of the substrates:

Substrate	H-binding energy (eV)	
	Atomic	Dissociative
Pt_Top	- 2.725	- 0.487
AuW_Hollow	- 2.194	0.033
RuW_Hollow	- 2.735	- 0.497
PdW_Hollow	- 2.406	- 0.168

All the negative values of dissociative energy prove that those structures are good for adsorbing hydrogen gas molecule and dissociate it into atomic hydrogen. The AuW with positive value dissociative energy means that it cannot facilitate hydrogen molecule dissociation. So, it cannot act as an anodic catalyst in fuel cell. We discarded this structure for our further calculation. So, we have the two structures RuW and PdW as the possible candidates of the electrocatalysts.

3.5.3 CO-tolerance:

The main objective of the paper is to look for the electrocatalyst mostly free from CO-poisoning that the pure Pt is highly affected from. We have come across many examples of electrocatalysts and ways of elevating the CO-tolerance. Here we define the CO-tolerance in terms of the rate at which the chemical reaction proceeds. The rate of reaction depends on the difference of Gibb's free energy and ultimately on binding energy of CO and OH on the particular substrate. We identified the active sites where the molecules (CO and OH) get adsorbed and calculated binding energies on the surfaces we've considered.

Table 3: Binding Energy of CO and OH on The Substrates and Preferred Sites.

Substrate	**Binding energy (eV)**			
	OH	**Preferred site**	**CO**	**Preferred site**
Pt	- 2.505	Top	- 1.751	hcp
Pd/W	- 3.306	Hollow	- 1.286	Bridge
Ru/W	- 3.467	Hollow	- 1.793	Hollow

Interestingly that OH is bound stronger on Pd/W than on Pt (111), while, CO binds weaker on Pd/W than Pt(111). This result is supposed to be favorable for lower CO poisoning. Ru/W looks behaving towards CO binding almost similar as Pt (111) does; however, OH is bound on Ru/W stronger than on Pt (111). The weakly bound CO on Pd/W is oxidized by OH to give out CO_2 to exit and H for oxidation.

From the above values, we calculated Gibb's free energy.

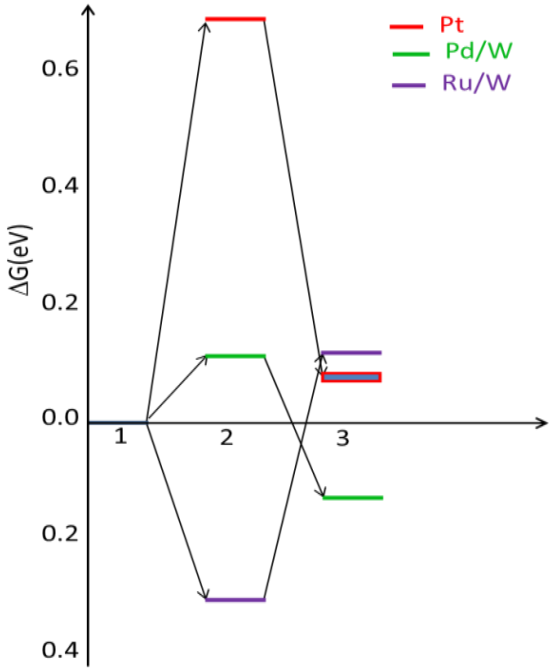

Figure 7: Free Energy diagram showing different pathways the reaction proceeds for different catalysts. First step represents the initial stage which is taken and the reference state, and the 3rd step represents the final stage. 2nd step represents the intermediate step (see the text below).

First step is uphill reaction for the Pt (111) and Pd/W while it is downhill for the Ru/W. The second step is downhill reaction for the Pt (111) and Pd/W while uphill for Ru/W. First step is the oxidation of H_2O to OH and H and second step is oxidation of CO to CO_2 in presence of OH. The first reaction is spontaneous in Ru/W while energy consuming for Pt (111) and Pd/W and in the second step vice versa. Second step is spontaneous for Pt (111) and Pd/W while energy consuming for Ru/W. It is seen that for the Ru/W, OH binds stronger and so the reaction proceeds spontaneously. And, Ru/W that

binds CO stronger than others, the reaction is energy consuming. The overall reaction is the combined effect of the two steps on the reaction.

The effectiveness of the catalyst can be explained in terms of the rate at which the reaction proceeds. We calculated the rate of uphill reaction for both Ru/W and Pd/W relative to Platinum.

$$\frac{R_{Pd\_W}}{R_{Pt}} = 2.799 \times 10^{9} \quad (3.4.74)$$

$$\frac{R_{Ru\_W}}{R_{Pt}} = 2.733 \times 10^{4} \quad (3.4.75)$$

It is found that the reaction occurs way faster in Pd/W than on Pt. This indicates that Pd/W acts as the better catalyst than platinum. It is clear from this observation that, for the catalyst to be better for the HOR minimizing, it must be binding CO weaker and OH optimum.

3.5.4 Why are CO Bound Weaker and OH Stronger in Pd/W than in Pt (111)?

This has drawn our attention because it is critical for CO removal, and we performed a complex studies of this effect.

3.5.4.1 Modification of Electronic Structures due to Hybridization of the Electronic States:

Electronic density of states (DOS) is the means to study the reactivity of an active material. Reactivity is higher for those materials which have higher DOS accumulated nearby the Fermi energy[24]. Reactivity of the material can be tuned by modifying the DOS[71]. One of the well-known ways to change the reactivity of transition metal is to modify the local density of states (LDOS) of the surface atoms that can be done by varying the material

composition[72]. We calculated the LDOS and found that s and p states are very small and only the d-states do contribute for the binding process

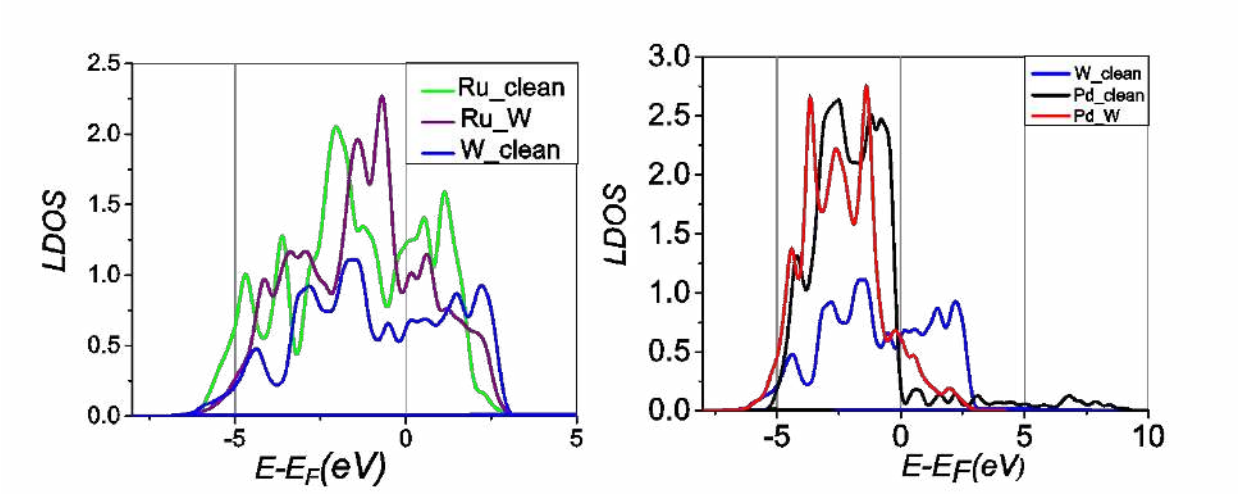

Figure 8: The LDOS of the clean surface of the substrate and then with the atomic layer on top of it. a) Clean Ru, W and RuW. b) Clean Pd, W and PdW.

We can see the appreciable modification of electronic structure at the interface because of M-W hybridization. When two d-states come into integration, the occupied states below the Fermi-level and the unoccupied states above the Fermi level hybridize and cause some modification of the electronic density of states distribution. This ultimately brings about change in reactivity of the material[72-73]. We cannot see appreciable difference in case of Ru/W, however, there is a big change in the LDOS around Fermi-level of Pd/W . The increase in unoccupied states in Pd/W and large decrease in occupied state might have changed the surface reactivity.

3.5.4.2 Shifting of d-Band Center:

D-band center is the average out of the density of states. Per d-band center theory, closer the d-band center is to the Fermi level; higher is the reactivity of the material[24, 73]. We calculated the d-band center of our structures.

Table 4: d-band center

S.N.		Pd (in eV)	Ru (in eV)
1	$M_{Element}$	Pd(111) = -1.269	Ru (0001) = -1.472
2	M/W	Pd/W (110) = -2.344	Ru/W (110) = -1.313

The table shows that the d-band center is shifted towards the lower energy level. It indicates that the reactivity is reduced. However, Ruthenium becomes more reactive. Moreover, we could see the shifting is larger in case of Palladium. It is concluded that, the d-band center theory cannot give the complete description of the electronic properties of these elements with narrowband structures[74]. In other words the d-band center theory cannot give accurate description of reactivity in all materials.

3.5.4.3 Charge Redistribution, Bader Analysis:

The charge distribution table shows that, in all the structures the substrate atoms (Pd) lose some charge density to the adsorbate. It is from Bader analysis that provides the scenario of the charge transfer between the atoms in the structure and an important explanation of bonding profile[27]. In case of OH, the charge absorbed from Pd resides with O atom to form bond with Pd. It is ionic bond which is stronger one[75]. However, CO takes

charge from Pd and keeps some with it and shares with O there by it forms a mixture of covalent and ionic bonding with Pd and between covalent bonding C-O. Since charge shared by C with O is bigger than that done with Pd, the covalent bonding C-O is stronger and bonding of CO with Pd is weaker.

Table 5: Charge transfer occurred between the atoms, Bader analysis:

<table>
<tr><th>Structure</th><th colspan="8">Charge (e^-)</th></tr>
<tr><td rowspan="3">OH_Pd_fcc</td><td colspan="4">Pd</td><td colspan="2">O</td><td colspan="2">H</td></tr>
<tr><td>17/21</td><td>18/22</td><td>19/23</td><td>20/24</td><td>OH_mol</td><td>OH_ads</td><td>OH_mol</td><td>OH_ads</td></tr>
<tr><td>15.851</td><td>16.032</td><td>15.836</td><td>15.843</td><td rowspan="2">6.977</td><td>7.472</td><td rowspan="2">0.000</td><td>0.000</td></tr>
<tr><td>OH_PdW_L</td><td>16.291</td><td>16.157</td><td>16.150</td><td>16.157</td><td>7.551</td><td>0.000</td></tr>
<tr><td rowspan="4">CO_Pd_hcp</td><td rowspan="4">15.924</td><td rowspan="4">15.934</td><td rowspan="4">16.015</td><td rowspan="4">15.949</td><td colspan="2">C</td><td colspan="2">O</td></tr>
<tr><td>CO_mol</td><td>CO_ads</td><td>CO_mol</td><td>CO_ads</td></tr>
<tr><td rowspan="2">2.097</td><td>2.308</td><td rowspan="2">7.871</td><td>7.906</td></tr>
<tr><td>CO_PdW_B</td><td>16.323</td><td>16.308</td><td>16.192</td><td>16.179</td><td>2.310</td><td>7.877</td></tr>
</table>

Figure. 9 below shows very little charge transferred to CO in Pd/W which is higher than in case of Pd itself.

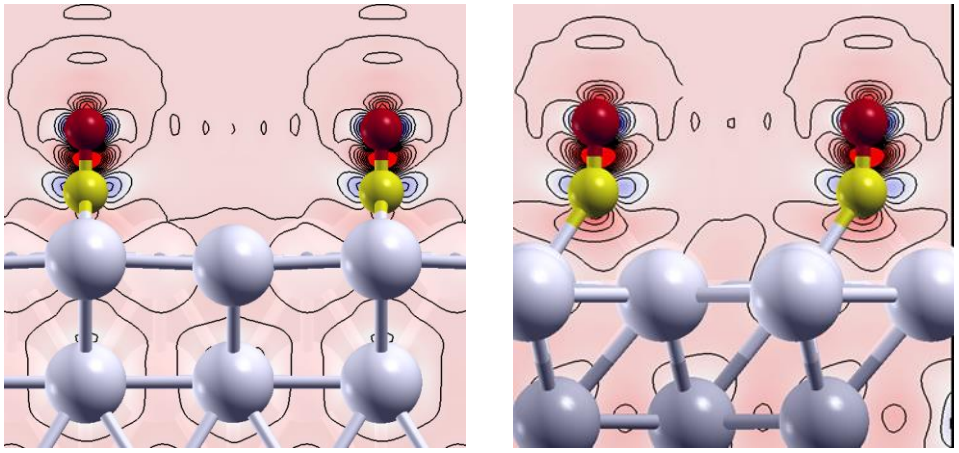

Figure 9: Charge redistribution with CO on Pd (light brown) and Pd/W;(W-dark brown).

3.5.4.4 Contribution of Different Mode Vibrational of Adsorbate.

The molecules CO or OH bound to the surface 'Pd' atom of the either structure Pd (111) or Pd/W vibrates in six different modes. Each mode contributes to the total vibrational energy. It is noteworthy that the higher vibration frequency is, the stronger covalent bond while changes in iconicity does not affect much the frequencies[76].

Table 6: Energy (hν) distribution for different modes of vibration.

Modes of vibration	Energy (eV)			
	OH_Pd_fcc	OH_PdW_H	CO_Pd_hcp	CO_PdW_B
OH, or CO stretch (1ν)	0.458	0.459	0.222	0.238
OH, or CO-Metal stretch (2ν)	0.051	0.059	0.042	0.037
Frustrated rotation (3ν)	0.051	0.051	0.042	0.033
Frustrated Translation (4ν)	0.041	0.041	0.039	0.029

From the comparison of modes of vibrations of OH on Pd (111) with Pd/W, we found that there is no any appreciable change in the contributions of modes of vibration for OH, however there is a lot change taking place in case of CO. CO stretched mode (1ν) is appreciably increased in Pd/W, however, C-Pd stretched mode is decreased. This indicates that the covalent bonding between CO is higher and bonding between C and Pd is decreased. That is in harmony with the result observed for charge transfer from Pd to CO. Moreover, diminished frustrated rotation and frustrated translation energy[42] indicate the weakening of the C-Pd bonding in Pd/W. The frustrated rotation is localized on the C atom attached to metal and it is lower on Pd/W than on Pd. The lower energy means lower is the frequency and weaker is the bonding. Since the frustrated translation is localized on the atom not bound with the substrate, which is O in case of CO, does not tell much about the bonding with metal, but the diminished value again shows the weakening of the bonding. This result confirms that C-substrate bonds of CO are more covalent than O-substrate bonds of OH.

3.5.4.5 Work Function

Ionicity of the adsorbate-substrate bond depends on the work function of the substrate: the lower the work function, the easier to transfer an electron from substrate to the adsorbate. We found the work function of Pd (111) 5.02eV which is quite close to previously reported value 5.25[77], 5.22[78] based on GGA, and 5.64[78] based on LDA and not far from the experimental value 5.90 ±0.01[79], 5.55±0.01[80] and for PdW we found 4.408 eV. The reduced work function of Pd when set on W(110) causes the stronger ionic binding of OH on PdW. Loosely bound electronic charge is taken by O in OH to form ionic bond. The electron affinity of oxygen is higher leading it to higher iconicity. Consequence is the stronger bonding of OH on PdW. Unlike this, C in CO has lower electron affinity prefers to form covalent bond with Pd. As seen in the table 6, charge that C takes from Pd in PdW would promote the ionic bonding. It means the bonding between the CO and PdW is mixture of covalent and ionic which is weaker compared to OH on PdW.

3.6 Conclusion

Based on the educated guess we selected three M/W(110) structures (M=Au, Ru, Pd) which we expected to be stable and might be promising electrocatalysts for hydrogen oxidation. Indeed, our calculation showed that all three structures are thermodynamically stable. Meanwhile we found that Au is not activated enough in Au/W to facilitate oxidation of hydrogen. Next, focusing on CO removal from the surface we calculated free energies for the removal reaction involving CO and OH adsorbed on the catalyst surface. We found that the removal of CO is not favorable on Ru/W, while it is much more favorable on Pd/W than on Pt. The reason for that is that CO adsorbs much weaker and OH much stronger on

Pd/W than on Pt. It happens because the reduced work function of Pd/W enhances ionic OH – Pd/W bonds, while it does not affect much the mostly covalent CO – Pd/W bond.

CHAPTER 4
RATIONAL DESIGN TECHNIQUE FOR FINDING PROMISING ELECTROCATALYST FOR OXYGEN REDUCTION REACTION

4.1 Introduction

Energy has been the topic of many fields of research. Reliable source of energy has been an ultimate goal of many researches. Fuel cell, a widely studied example is Proton exchange membrane fuel cell (PEMFC), is a device to convert chemical energy stored in Hydrogen molecule to electrical power. It functions by combining the hydrogen molecule introduced in Anode and Oxygen molecule introduced in cathode. Hydrogen Oxidation Reaction, [HOR] taking place in anode supplies Hydrogen ion and heart core reaction takes place in cathode called Oxygen Reduction Reaction, ORR. In both reactions, widely used catalysts are Pt and Pt-based materials, however, a number of obstacles are providing limitations to its large scale application of the fuel cell. First limitation comes from the cost of the rare and very expensive element Pt. Second limitation comes from the relatively low rate of ORR, that lowers the onset potential (~0.9 eV [SHE], that is 73 % of the ideal value 1.23 V [SHE]) and thus lowers the efficiency of the fuel cell[81]. So the search for the cheap and efficient catalysts as active as Pt or even better is of great interest and there have been researches in many directions to meet the goal. In this chapter, we implement the rational design technique to look for the materials promising catalyst for ORR.

4.2 Overview of the past works and our effort

One of the most effective directions is to lower the cost by reducing the load of Pt or Pt-group materials in the electrocatalytic system used. Adzic's group has come up with some progress in setting up the monolayer of Pt on Pt-alloy substrates[82-86] and have shown by combining experimental and first principle calculations that some Pt-M structures have higher ORR activities compared to that on bulk Pt.

Authors of Zuluaga and Stolbov[87] in their comparative studies of the reactivity of pure $Pd(111)$ and alloy Pd_xCo_{1-x}, have reported that hybridization of dPd and dCo electronic states to be the main factor controlling the electrocatalytic properties of the later structure. They have compared the reactivity with different concentrations and shown that the low shift of surface dPd states with respect to the $Pd(111)$, weakens the bonding between the ORR intermediates and the $Pd_x\ Co_{1-x}$ surface making it favorable for ORR. They have reported that there is a little change in bonding and hence the rate of ORR reaction due to the presence of water molecules.

Successful attempts have been seen in developing the core-shell nanoparticles with Pt shell and Pt-Fe, Pt-Co, Pd_Fe, Ir-Co cores[82-86, 88-89].The shortcoming of these designs is that they still make the use of large fraction of the Pt or Pt-group elements, they can reduce only 20% of Pt so far.

Some researchers have argued with the use of graphene doped with some atoms as the promising electrocatalyst for ORR. Studies have shown that without modification, the single atom carbon sheet is very inactive because of the low binding of oxygen reduction intermediates [90-92]. The hybridization of carbon and the metal atom electronic states makes

the structure promisingly active of the ORR. Xen Chen's group[93] has studied ORR performance of 10 different kinds of metal-doped-Graphene M_G with M = Al, Si, Mn, Fe, Co, Ni, Pd, Ag, Pt and Au. On confirming chemical stability of these structures, they have shown that the linear relation of the binding energies of the ORR intermediates that found in metal-based materials does not hold in such structures and hence a single binding energy of intermediate alone is not sufficient to evaluate the ORR activity of an arbitrary catalyst. They have recommended Au-, Co- and Au-G materials as the potential electrocatalysts for ORR. No structure has been found that can surpass the activity of Pt[93], however, Au-G has been reported to have activity more than that of Pt[94].

Recent researches have pointed out an intrinsically conductive metal-organic frameworks [MOFs] on cheaper material to be durable and structurally well-defined catalyst for the ORR[95]. MOFs are crystalline, Nano-porous materials composed of metal ions linked with by coordination bonds to organic electron donors. The platinum free complexes look in the form of MN_x where M = metals such as Fe, Co, Ni coordinated with Nitrogen that has to be mixed with the Carbon in the electrode to ensure conductivity[96]. Recently, designed two dimensional layered structure analogous to graphene, designed as a 'metal-organic graphene analogue'[97].Mentioning about the shorting the knowledge of the structural mechanism and durability of the MOF film on glassy carbon surface it is reported that the reduction of Oxygen molecule takes place with an onset potential of 0.82 V (RHE), similar to the most active non-platinum group ORR catalyst. The design is yet to be implemented to 4 electron ORR reactions.

Next challenge in developing the electrocatalyst is its stability in the acidic environment at the electrode potential which is expected to be in efficient fuel cell. Elements will dissolve if their dissolution potential is lower than the working potential of the cell. Pt, Au and Ir are few examples of stable materials, however, Ir is less abundant than Pt and Au is too noble. Durability issue of Pt itself is critical in low pH scale environment[98]. Meanwhile, Pd has been reported as the good candidate for catalyzing ORR as it has dissolution potential at pH = 0 to be Pd = 0.95[99], higher than the operational potential of Pt-based cell. This is the reason why the Pd has been studied extensively[100].The fact that its stability is improved as a catalyst designed is in a form of monolayer on top of more reactive alloy surface.

Not a single catalyst works for all, and a single method is just enough to identify the proper catalyst. A radical and new approach is needed; Rational Design Principle [RDP] is introduced as the best option. Preselection of the system of materials from the knowledge of nature of the materials is helpful in designing catalysts. RDP is the method of tuning of the catalytic behavior of the material by the modification of the surface composition and/or morphology. Such method is guided from the understanding of the relationship among the surface composition, electronic structure, reactivity and energetic activity towards ORR. The main aim of this work is to dig into the details of that relationship based on the existing pieces of knowledge on the correspondence between them[62, 101].

As the catalytic properties are determined by the binding energies[94], designing the highly active ORR catalyst requires the ability to tune the binding energy of the

intermediates on the catalytic surface. We look for the appropriate composition and structure of the catalyst that can display the desired binding energies. Our approach to rational design of catalyst proceeds with selection of only promising materials based on the knowledge of the composition and the properties unlike the computational screening of hundreds random compositions. First principle calculation is performed to test and narrow down the selected materials. Then the design is experimented for the best candidate of the catalyst.

In our system, we took 5-layer of slab element (SE = Nb and Mo) and monolayer of active elements (AE = Pt and Pd) is formed on top of it. The stability of the FCC base monolayer set on the BCC base slab is tested first. The hybridization of the $d\ band$ of the Pd element hybridizes with the $d\ band$ of the slab element enhancing the ORR activity. Such activity has not been done in Pd/Nb and Pd/Mo yet.

Binding energies are calculated for each intermediates on the AE surface in appropriate site. Our first participle calculation shows that the binding energy of O, OH and OOH are the descriptors of the ORR and we could express a linear relationship between the binding energy and the Gibb's free energy of the form:

$$\Delta G = E_B + \alpha \tag{4.1.76}$$

Where 'α' is a constant that comprises the ZPE and entropic contribution which are either constant or vary very negligibly over different catalysts.

However, we see from the DOS calculation that the activity and the d-band center model is not accurate as it could not describe the activity of the catalyst we've considered. From the Rational Design approach, we had selected four different candidate structures

PtMo, PtNb, PdMo and PdNb for the calculation. We found that first two behaving approximately same as Pt while rest of the two are worse We could reveal that the main factor controlling the ORR rate is the binding of O, OH and OOH on the catalyst. It is one step forward in identifying the possible electrocatalyst for the ORR.

4.3 Methods:

4.3.1 ORR Thermodynamic Model:

ORR is a complex multi-electron exothermic reaction that may go through many intermediate steps. As summarized in the article by Adzic[102], mainly two pathways are possible for the reaction as described below:

1. Direct four electron reduction pathway:

   The oxygen molecule undergoes reduction completely in the combination with the free proton and electron to yield water molecule.

$$O_2 + 4H^+ + 4e^- \rightarrow 2H_2O \quad (4.2.77)$$

2. Peroxide pathway:

   The oxygen molecule reduces to water molecule in two steps with the hydrogen-peroxide as the intermediate product:

$$O_2 + 2H^+ + 2e^- \rightarrow H_2O_2 \quad (4.2.78)$$

$$H_2O_2 + 2H^+ + 2e^- \rightarrow 2H_2O \quad (4.2.79)$$

The second step in path way 2 has very high reversible potential that reduces the efficiency of ORR significantly. As the ORR is the heart of operation of fuel cell, there has been extensive study and a lot of catalyst has been tested so far. It has been suggested that for

the Pt[102] and such ORR active catalysts[86, 103], the 4-elctron pathway is predominated. DFT based calculation shows that the activation barrier of O_2dissociation is very high and hence the molecular adsorption on the catalysts' surface is favored. The process proceeds through the following steps:

$$O_2 + * \longrightarrow O_2^* \tag{4.2.80}$$

$$O_2^* + (H^+ + e^-) \longrightarrow * OOH \tag{4.2.81}$$

$$* OOH + (H^+ + e^-) \longrightarrow H_2O + O^* \tag{4.2.82}$$

$$O^* + (H^+ + e^-) \longrightarrow HO^* \tag{4.2.83}$$

$$HO^* + (H^+ + e^-) \longrightarrow H_2O + * \tag{4.2.84}$$

Where '*' denotes the adsorption site on the catalysts surface. We calculate the change in free energy ΔG for each intermediate state by taking the final state of the reaction to be clean catalyst surface plus H_2O in gas phase which is practically zero[94].

As the reaction steps involve transfer of charge, the contribution of the transferred proton across the electrodes to the free energy 'G' is determined as $G_U = -neU$ where U is the electrode potential and n is the number of proton transferred while the reaction proceeds from the particular intermediate state to the final state.

As a result, for each ORR intermediate state, the change in free energy is defined as:

$$\Delta G = \Delta E + \Delta ZPE - T\Delta S + \Delta G_U \tag{4.2.85}$$

Here, ΔE is the internal energy of the catalyst surface with an intermediate adsorbate and is obtained by DFT calculation. The total energy of the intermediate adsorbed on the catalyst surface is calculated w.r.t to the total energy of the final state and the binding energy of the intermediate adsorbate E_B as shown below:

$$\Delta E(O) = E_{tot}(H_2) + E_{tot}(O) - E_{tot}(H_2O) - E_B(O^*) \quad (4.2.86)$$

$$\Delta E(OH) = \frac{1}{2}E_{tot}(H_2) + E_{tot}(OH) - E_{tot}(H_2O) - E_B(OH^*) \quad (4.2.87)$$

$$\Delta E(OOH) = \frac{3}{2}E_{tot}(H_2) + E_{tot}(OOH) - 2E_{tot}(H_2O) - E_B(OOH^*) \quad (4.2.88)$$

ΔZPE is the zero-point energy correction obtained that depends on the vibration frequencies. It was obtained by DFT based calculation which is carried out by allowing the adsorbates vibrate keeping the substrate frozen. The entropic contribution $T\Delta S$ is determined for the gas phase of the adsorbate which is based on the data obtained from CODATA[68] that does not vary with the substrate. Since adsorbed molecules do not have translational and rotational degrees of freedom, their entropic part is small and neglected in our calculations. Therefore, in a good approximation the variations of free energy diagram from one surface to other is mostly determined by the binding energies of O, OH and OOH.

The strength of binding of intermediate $'X'$ on the substrate is defined as:

$$E_B(X) = E_{tot}\left(\frac{X}{Sub}\right) - E_{tot}(X) - E_{tot}(sub) \quad (4.2.89)$$

Where E_{tot} term denotes the total energy per super cell and the X, represents the adsorbate and the sub refers to the substrate.

With the DFT result of the ZPE that does not vary much from material to material and the observed entropic contribution which is constant for a structure, we could derive the simplified version of equations above in the following form:

$$\Delta G(O) = E_B(O^*) + a \quad (4.2.90)$$

$$\Delta G(OH) = E_B(OH^*) + b \quad (4.2.91)$$

$$\Delta G(OOH) = E_B(OOH^*) + c \quad (4.2.92)$$

Where a, b and c denote the ZPE and the entropic contributions.

4.3.2 Computational Details:

All our DFT calculations are performed using Vienna ab initio simulation package, VASP5.2 code[66] with the projector augmented wave psudopotentials[104] with the Perdew-Burke-Ernzerhof (PBE) parameterization for the exchange and correlation functional[17]. In order to maintain the periodicity, we use the supercell that includes the 5 layers of slab of Nb or Mo, one layer of Pt, or Pd with 1x1 periodicity and ~ 14 Å vacuum layer which is assumed to be avoid the interaction between the slabs. The 8 x 6 x 1 k-point grid in Brillouin zone is used for integration in the reciprocal space. The cut off energy of 500 eV is used for the plane wave expansion of the wave function and the charge density which is sufficient to converge the total energy for the given k-point sampling. The atomic relaxation was carried out until the force acting on each atom and in each direction does not exceed 0.001 eV/ Å.

The xcrysden software[70] was used to plot the geometric structures of the system under consideration.

4.4 **Result:**

4.4.1 Stability of the Catalyst:

4.4.1.1 Thermodynamic Stability:

It is important to test at first whether the physical structure is favorable to be formed and stable to exist. As we are looking for the cheaper catalyst we look for the active element as a monolayer on top of the cheap substrate element. In this regard we see mainly 3 different aspects. First, we have chosen fcc type of AE and bcc type of SE. There is lattice pattern mismatch between the monolayer and the substrate. We have to looks for the material having less bond-length mismatch to avoid the strain. Second, the binding of the atoms of AE and SE must be greater than the AE-AE atoms $E_B(AE\_SE) > E_B(AE\_AE)$, otherwise the AE atoms collect together to form the 3D clusters. Next, is the cohesive energy of the substrate $E_B(SE\_SE)$ has to be greater than the binding energy of the AE and the SE, $E_B(AE\_SE)$; this prevents tunneling of AE atoms giving rise to the alloying of the two materials.

In our system, we take Pt and Pd as the active elements and 5 layered slab of Nb and Mo as the substrate. As the formation energy of each AE-SE (AE = Pt, Pd and SE= Nb, Mo) is higher than that of AE-AE, there is possibility of formation of the AE monolayer of the selected AE on both material slabs. Table below confirms the statement. The pictures aside provide the visual structure.

Table 7: Binding energy of the monolayer per atom on the slab, cohesive energy of the active elements and the Formation energy.

Structure	Pt/Nb	Pt/Mo	Pd/Nb	Pd/Mo
$E_B^{AE-SE}(eV)$	-7.141	-6.982	-6.305	-5.762
$E_{Cohesive}^{AE-AE}(eV)$	-5.850	-5.850	-3.920	-3.920
$\Delta E_{form}(eV)$	-1.291	-1.132	-2.385	-1.842

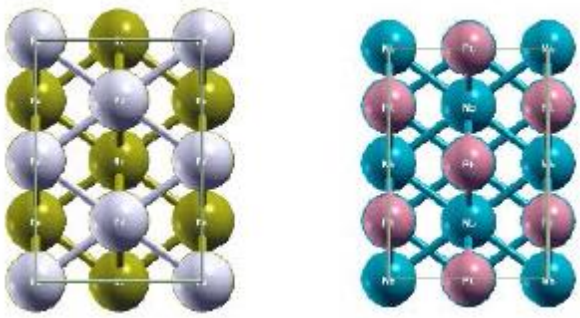

Figure 10: Structure of monolayer of Pd (left Silver) on top of Mo slab and Pt (right Red) on top of Nb slab.

Since the FCC structure of AE is set on the top of BCC structure of slab of both Nb and Mo, there would be some kind of lattice mismatch and a strain in the few layers on the surface. The materials are having almost same bond length, so, the physical strain can be neglected. However, there would be some changes in electronic properties and hence the catalytic actions, that would be accounted in DOS calculation. We look for such a combination that is stable and promotes the ORR.

Table 8: Bond length of the monolayer elements Pt and Pd and the slab elements Nb and Mo.

Elements	Pd	Pt	Nb	Mo
Bond length (Å)	2.8143	2.8072	2.8795	2.7449

From the table 2, we can see that the monolayer active elements Pd and Pt have bond lengths not much different from the slab elements, Nb and Mo. So, we can expect less strain effects in the structures. The, fact is in support of the stability of the structure. 1) These elements are inexpensive and highly abundant in the Earth's crust. 2) The chosen MS elements have bcc structures, for which the (110) surfaces have the lowest surface energies, and, hence, the (110) facets in nanoparticles have the highest area fraction. 3) These metals have a very small bond-length mismatch with the elements chosen as candidates for AE, which is a necessary condition for stability of the AE/MS structures. Indeed, an Au monolayer will fit well to Nb and Ta surfaces (only 0.9% contraction), and will be ~5.6% contracted on Mo and W. Pt-Pt and Pd-Pd bonds will be expanded on Nb and Ta surfaces by ~3.6% but fit almost perfectly on Mo and W surfaces.

4.4.1.2 Electrochemical Stability:

a. Dissolution of the Catalyst in Acidic Medium:

Another aspect of choosing the catalyst is the chemical stability of the cathode electrode in the acidic medium inside the cell. Most materials having dissolution potential $U_{diss,}$ lower than the operational potential (that created when the power of the fuel cell is maximum) of the fuel cell, will disintegrate and dissolve, so, cannot be used as the catalyst..

In practice, the problem is even severe as the dissolution potential is set in lower level than the nominal one. In acidic (pH = 0) medium the dissolution of Pt sets in an electrode potential of 0.65 V instead of nominal 1.18 V one and that is much lower than the operating potential of the efficient fuel cell.

An efficient fuel cell is supposed to work at the potential of,$U > 0.7\,V$. We've chosen such materials which can survive in such environment. Both Pd and Pt have dissolution potentials higher than the operation potentials of the cell. There are very few materials having U_{diss} higher than the operating potential that would of the efficient fuel cell ~ 0.8 - 1.0 V (SHE): U_{diss} of Ir, Pt and Au are 1.16, 1.18 and 1.5 V (SHE) respectively[99]

Table 9: Dissolution Potential of some common elements. [Ref.]

Metal	**Fe**	**Co**	**Cu**	**Ru**	**Rh**	**Ag**	**Pd**	**Ir**	**Pt**	**Au**
$\boldsymbol{U_{diss}}$ (V vs. SHE, at pH = 0)	- 0.45	- 0.28	0.34	0.46	0.60	0.85	0.95	1.16	1.18	1.50

It is seen that the Pd, Ir, Pt and Au are some elements that survive in the acidic environment of the fuel cell electrolyte. These should be good candidate of catalysts for ORR in the cathode electrode. We've chosen two of the most stable elements, Pt and Pd for the structure of our consideration.

Dissolution potential of the monolayer material depends on the dissolution potential of the individual element and formation energies of the composite materials as represented by the equation[105] :

$$U_{diss}\left(\frac{AE}{SE}\right) = U_{diss}\left(AE_{element}\right) + \left(E_{form}\left(\frac{AE}{SE}\right) - E_{form}\left(\frac{AE}{AE}\right)\right)/n_{diss}e \quad (4.3.93)$$

From this expression it is seen that the dissolution potential can be tuned be selecting the suitable combination of the AE and SE. For an element chosen for the fuel cell the dissolution potential, $U_{diss}\left(AE_{element}\right)$, is at least positive. $U_{diss}(AE/MS)$, thus can be increased by choosing the materials such that $E_{form}\left(\frac{AE}{SE}\right) > E_{form}\left(\frac{AE}{AE}\right)$. Table.10 Shows that the dissolution potential of all AE/SE (AE = Pt, Pd and SE = Nb, Mo) is elevated.

Table 10: Dissolution potentials of the structures we have considered.

$\frac{AE}{SE}$	$\frac{Pt}{Mo}$	$\frac{Pt}{Nb}$	$\frac{Pd}{Mo}$	$\frac{Pd}{Nb}$
$U_{diss}\left(\frac{AE}{SE}\right)$	1.75	1.83	1.87	2.14

All the structures can survive in the acidic environment in cathode compartment of the cell.

b. Electronic Structure and Catalytic Activity:

As the monolayer is formed on the substrate, the electrochemical activity will be changed. The hybridization of the d-states of the monolayer atoms and the substrate atoms brings about the change in density of states distribution and consequently the change in reactivity of the structure. That property is implemented in describing and selecting the catalysts for the fuel cell. We calculated the LDOS of the surface atoms of the monolayer and nearby atoms of the slab. However, the plots below show that the d-band center model is inaccurate as it cannot tell much about the reactivity of the structure.

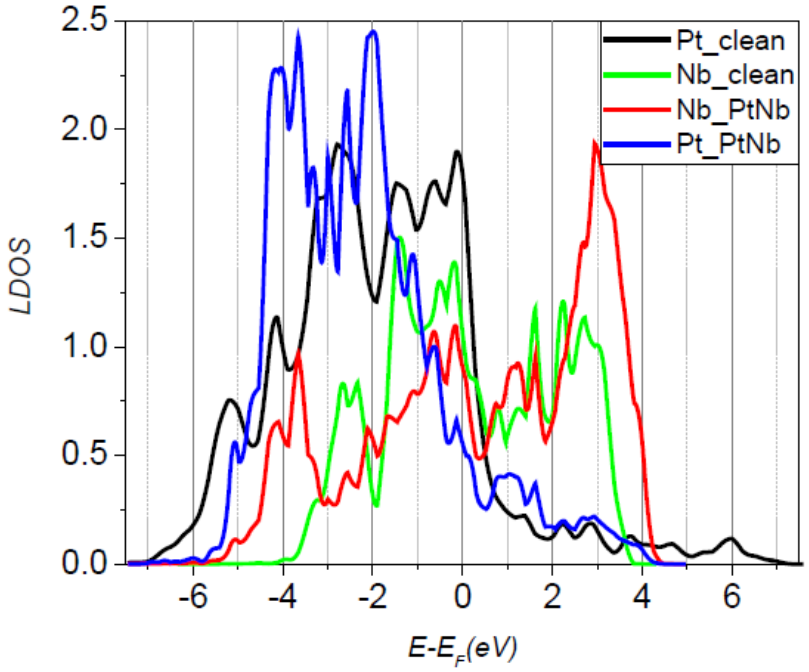

Figure 11: LDOS of the clean Pt (black), clean Nb (green), monolayer Pt in PtNb (blue) and Nb atom in PtNb(red).

The plot shows a slight modification of LDOS of Pt after setting its monolayer on Nb.

However, it does not provide strong basis to understand how the reactivity changes.

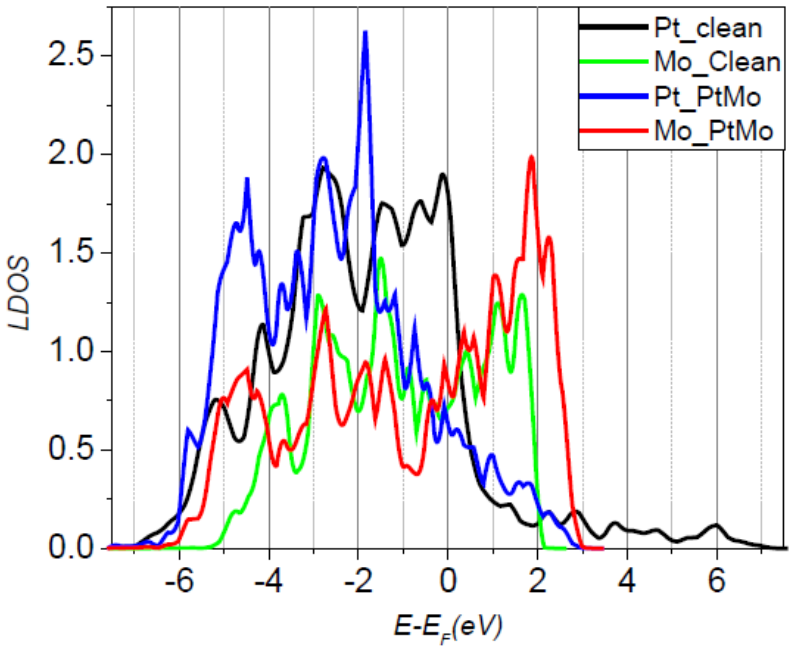

Figure 12: LDOS of the clean Pt (black), clean Mo (green), monolayer Pt in PtMo (blue) and Mo atom in PtMo(red).

We can see little modification of LDOS Pt when set as monolayer on the top of Mo-slab. It is hard to draw any conclusion how the reactivity of the structure changes

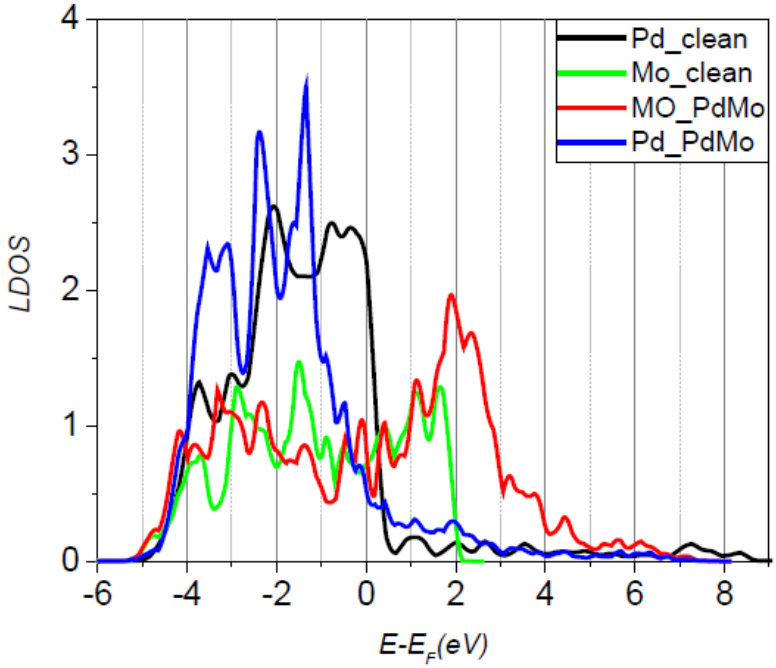

Figure 13: LDOS of the clean Pd (black), clean Mo (green), monolayer Pd in PdMo (blue) and Nb atom in PdMo(red).

There is slight change in LDOS of Pd cannot provide information about how the reactivity of Pd on Mo slab.

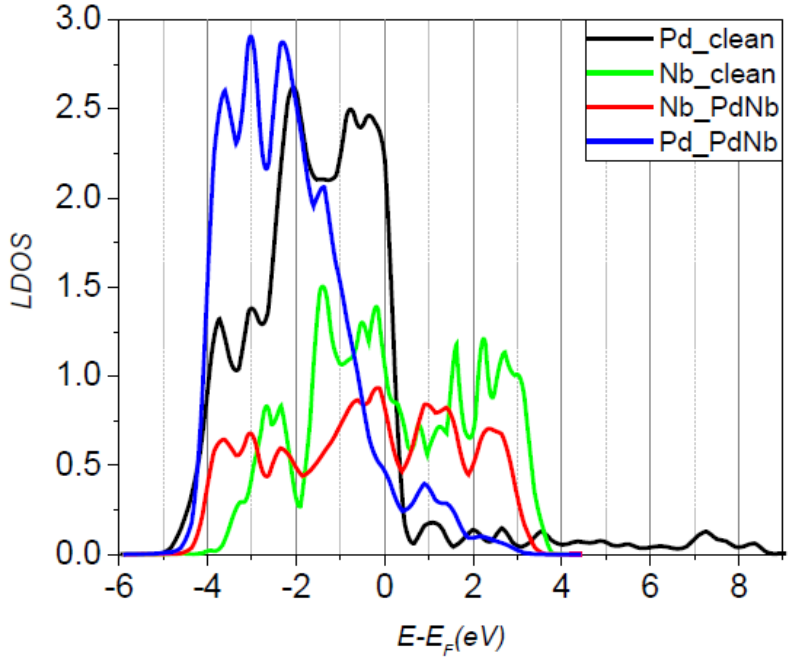

Figure 14: LDOS of the clean Pd (black), clean Nb (green), monolayer Pd in PdNb (blue) and Nb atom in PdNb(red).

This plot shows a little change in LDOS of Pd when set as a monolayer on top of Nb-slab, however, it is not evident to explain how the reactivity of Pd changes.

The conclusion of this discussion of the plots is that the LDOS is not sufficient to project the reactivity of the materials in our case. We need more information to understand it..

4.4.2 Thermodynamics of the Oxygen Reduction Reaction:

To illustrate the ORR activity of different catalysts we build ORR free energy diagrams. As shown in theory section, free energy is contributed by the total energies through the biding energy of the adsorbates. It is important to note that the intermediate products O, OH and OOH are the descriptors of the ORR activity.

We first determined the preferred site in the catalyst by calculating the binding energy of each adsorbate. O binds in right hollow site and bonds are formed from the hybridization of Px, Py state with dx, dy components of the AE atoms. Interestingly, O in PdNb form one extra bond with the Nb atom too. In the same way, OH prefers to stay in Bridge site and OOH on Top site. We calculated the binding energy of each intermediate product in the preferred sites of the catalyst. It is notable that the binding energies of the intermediate products are found to be in the order favorable for the ORR i.e.$E_B(O) > E_B(OH) > E_B(OOH)$ which is same as that reported for the Pt- and Pd-based ORR catalysts[62, 69, 87], however, the amounts differ for different metals.

Table 11**: Binding energies and ZPE of three different adsorbates O, OH and OOH in the different structures.**

Adsorbate	***O***			***OH***			***OOH***		
Structure	Site	$E_B(eV)$	ZPE (eV)	Site	$E_B(eV)$	ZPE (eV)	Site	$E_B(eV)$	ZPE (eV)
Pt	fcc	−4.157		Br	−2.394		Top	-0.965	
PtNb	Hollow	-3.966	0.063	Br	-2.414	0.349	Top	-0.964	0.429
PtMo	Hollow	-3.975	0.056	Br	-2.522	0.352	Top	-1.026	
PdNb	Hollow	-4.643		Br	-2.647		Top	- 0.322	
PdMo	Hollow	-5.741		Hollow	-4.326		Top	-2.778	

Another contributor of the free energy, the Zero Point Energy [ZPE], is calculated by calculating energy associated with all the modes of vibration of the adsorbate. Calculation

shows that ZPE in all intermediate products adsorbed on the catalysts are found not to be changing with the catalyst surfaces so we implemented the average value for developing the general equation for free energy calculation. For entropic effects we refer the data from the CODATA[68].

Free energy is calculated for each intermediate steps of the reactions by taking the final product, H_2O, as the reference 'zero' level. From, overall calculation, we obtained the value of constants a, b and c in equations 4.2.90 - 4.2.92 4.2.914.2.91 and hence found the relations as below:

$$\Delta G(O) = E_B(O^*) + 5.403892 \quad (4.3.94)$$

$$\Delta G(OH) = E_B(OH^*) + 3.036225 \quad (4.3.95)$$

$$\Delta G(OOH) = E_B(OOH^*) + 4.230887 \quad (4.3.96)$$

We have corrected notion of widely used combinatorial screening of metal/alloy surfaces as possible candidate for ORR catalyst that calculation of $E_B(O)$ is not sufficient to evaluate activity of any arbitrary material towards ORR but $E_B(OH)$ and $E_B(OOH)$ are essential too[94].

In the next, we build the ORR free energy diagram for all the structures we considered for zero electrode potential i.e. $\Delta G_U = 0$ and at the calculated onset potential of Pt (0.62 V)

From fig. 15, it is seen that stronger binding of the OOH molecule in PtMo slightly shifts the energy down but the weaker binding of O pulls it up above than that in the case of Pt. again stronger binding of OH again costs more energy and pushes the level down so that there could be a little endothermic uphill reaction. But the overall reaction profile

shows that the PtMo behaves almost same as Pt does. Here the binding of OH determines the limiting value of the potential that the cell can drive the current, the onset potential and it is equal to that of Pt, 0.62 V

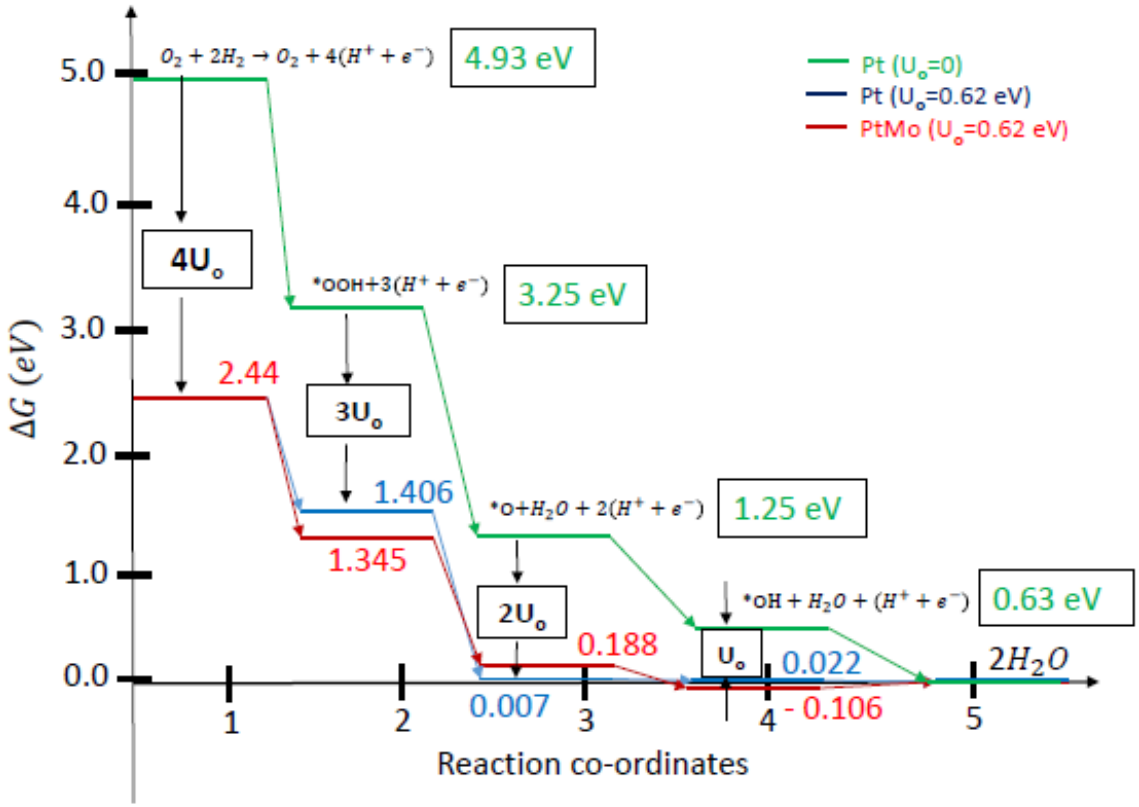

Figure 15: 4 electrons transfer ORR reaction energy diagram with $Pt(U_o = 0)$, $Pt(U_o = 0.62)$, and $PtMo(U_o = 0.62)$.

Fig. 16 shows that in PtNb, OOH binds almost same as on Pt. The consequence is the in first reduction step the energy stays almost as that of Pt, however, weaker binding of O leaves the energy level after second reduction step a bit higher than that of Pt. Molecule in PtNb that shifts the energy down a little bit but the weaker binding of O pulls it up above than that in the case of Pt. again stronger binding of OH again costs more energy and pushes

the level down so that there could be a little endothermic uphill reaction. But the overall reaction profile shows that the PtNb behaves almost same as Pt does. Here the binding of OH determines the limiting value of the potential that the cell can drive the current, the onset potential and it is equal to that of Pt, 0.62 V

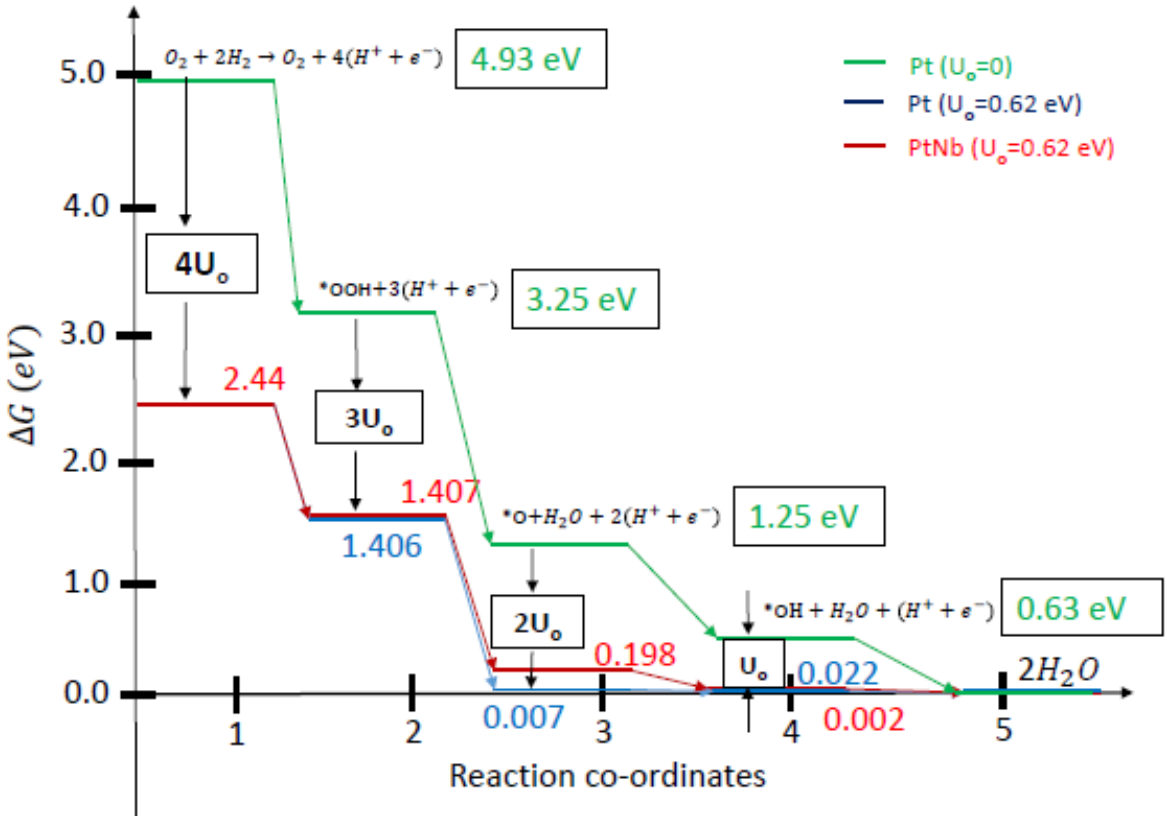

Figure 16: 4 electrons transfer ORR reaction energy diagram with $Pt(U_o = 0)$, $Pt(U_o = 0.62)$, and $PtNb(U_o = 0.62)$.

Fig. 17 below shows the catalystic action of dNb. Relatively weakly bound OOH will find sufficient life time to react with the H^+ to react to yield the next step. However, the strongly bound O pushes the energy level down to the negative values and provide significant barrier to the reaction. Binding of OH is not so high so, the energy gets lifted up a little bit. Because of the uphill

reaction processes, the ORR reaction is not found to be effective and the catalyst is not suitable for the ORR reaction of fuel cell.

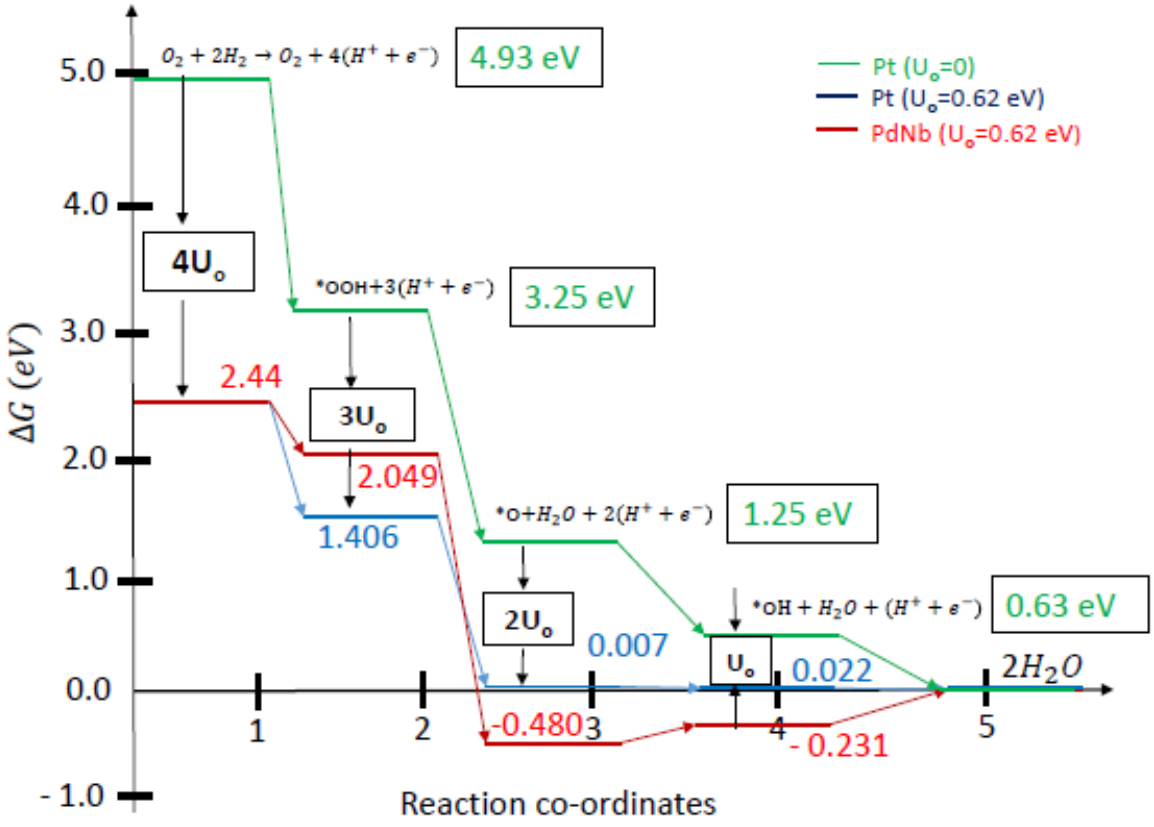

Figure 17: 4 electrons transfer ORR reaction energy diagram with $Pt(U_o = 0)$, $Pt(U_o = 0.62)$, and $PdNb(U_o = 0.62)$.

Similarly, the fig 18 below shows that in PdNb, the Strongly bound all of the intermediates OOH, O and OH push the energy level so deep that there would be required a lot of energy to lift it up and reaction is very hard to proceed. The conclusion is that the ORR reaction is almost impossible to proceed and the catalyst PdNb does not work for the ORR reaction of fuel cell.

The remaining part of the issue is to explore why there is difference in binding of the radicals in different surfaces.

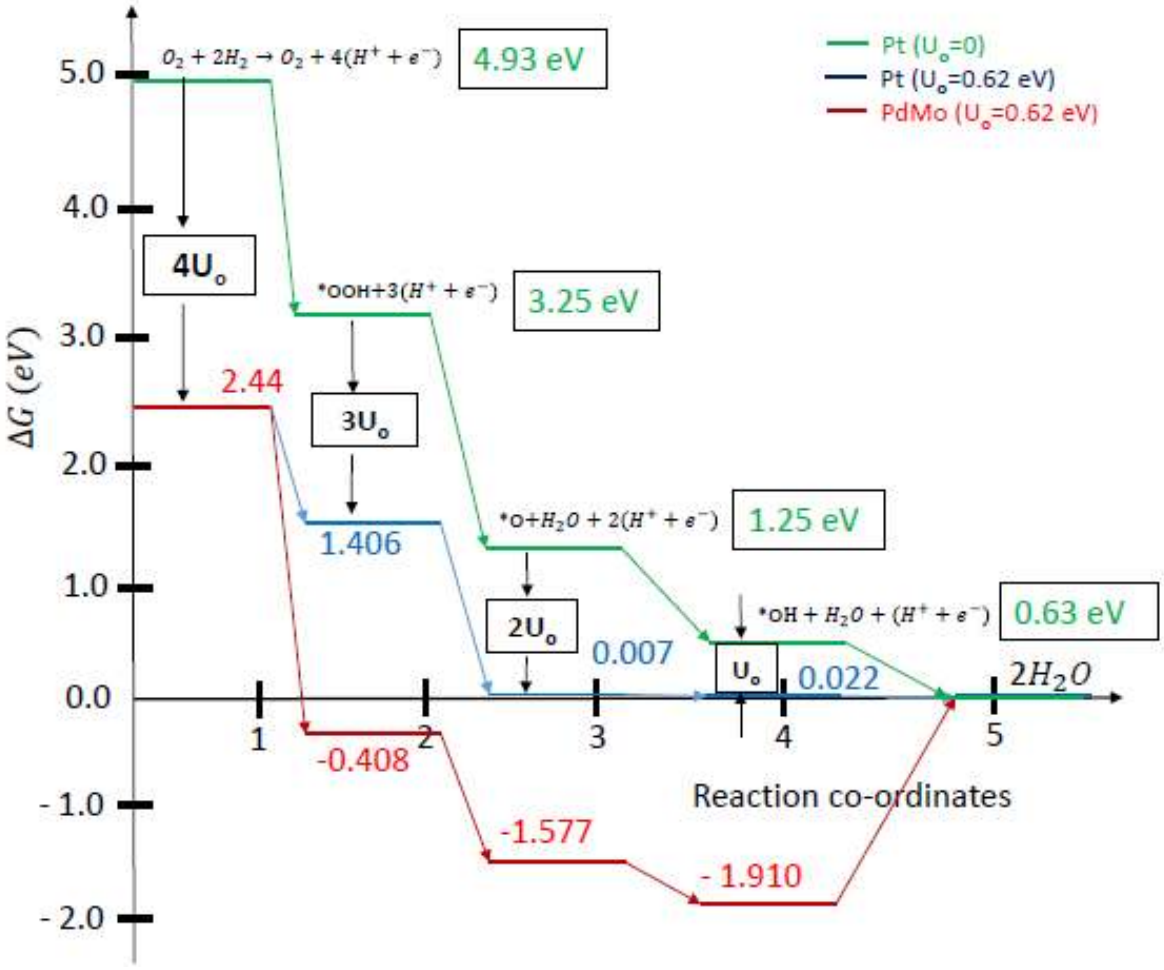

Figure 18: 4 electrons transfer ORR reaction energy diagram with$Pt(U_o = 0)$, $Pt(U_o = 0.62)$, and $PdMo(U_o = 0.62)$.

4.5 Conclusion

Searching for promising candidates for ORR catalysts we applied the educated guess to preselect stable and inexpensive materials which were expected to facilitate ORR. The structures were Pt/Mo(110), Pt/Nb(110), Pd/Mo(110), and Pd/Nb(110), denoting Pt or Pd monolayer on the Mo or Nb surfaces. Our calculations showed that indeed, consistently with our hypothesis, all these materials have to be thermodynamically and electrochemically stable. Attempts to link the obtained binding energy of the ORR intermediates to LDOS did not show much correlation between LDOS of surface atoms and surface reactivity, confirming that d-band model does not work for complex structures. We calculated free energies of the intermediate and final states for the systems in consideration and found that two materials – Pd/Mo and Pd/Nb hardly facilitate ORR. Meanwhile, the calculated ORR onset potential for Pt/Mo and Pt/Nb is found to be very close to that of Pt, which suggest that these two materials can be promising ORR catalysts which should be tested in experiment.

CHAPTER 5
ON THE ELUSIVE LINK BETWEEN ADSORBATE'S BINDING ENERGY AND BOND STRENGTH: AN ILLUSTRATION FROM CO ADSORPTION ON METAL DOPED GRAPHENE.

5.1 Introduction

Heterogeneous catalysis and electrocatalysis are widely used in numerous technologies. Nonetheless, there are challenging issues to resolve to make catalysts more efficient and/or to reduce their cost. For example, the prohibitive cost and relatively low stability of Pt-based electrocatalysts is currently hindering the commercial application of hydrogen fuel cells.

Rational search for efficient catalysts demands control and thus information about the kinetics of the desired reaction, however, knowledge of the *reaction thermodynamics* remains the first and foremost piece of information we need to obtain about any catalyst in order to assess its suitability[69, 94]. Indeed, if for a given material the free energy ΔG (which is given with respect to some reference energy) of any intermediate or final state of a reaction is higher than the ΔG of the initial state, then such material definitely cannot facilitate efficiently the reaction *regardless of the height of the kinetic barriers*. Another reason for which the reaction thermodynamics is essential is that it determines the *onset potential*. This parameter fairly characterizes the efficiency of electrocatalysts and can be estimated by analyzing the free-energy diagram that is obtained out of the reaction thermodynamics.[69] As such, the focus is on the ΔG each one of the states through which the desired reaction takes place. The ΔG of any reaction state can be obtained as:

$$\Delta G = \Delta E + \Delta ZPE - T\Delta S \quad (5.1.97)$$

ΔE is the ground-state internal energy of the catalyst surface adsorbed with an intermediate reactant/product. ΔZPE is the zero-point energy, and $T\Delta S$ is the entropic contribution. ΔZPE and $T\Delta S$ may be considerable, but their changes from one catalyst to another are negligible, for which they do not play an important role on improving the relative efficiency of a catalyst. ΔE on the other hand can change significantly from catalyst to catalyst. Importantly, the ΔE of a reaction state ΔE is determined by the binding energy E_B of the corresponding reaction intermediate reactants/products and the total energy of the free molecules related to that state[69, 87]. Therefore, the E_B of the adsorbed species involved in the reaction entirely determine the relative differences among the reaction thermodynamics of possible catalysts and thus their efficiency.

Since the catalytic activity of a material depends on the reaction thermodynamics, a critical aspect in designing a highly active catalyst is the ability to tune the E_B of the reaction reactants, intermediates, and products on the catalyst surface. Currently, since Density Functional Theory (DFT) total-energy calculations allow for obtaining binding energies relatively fast and inexpensively, some research groups try to find efficient catalysts by computational testing hundreds of materials (the high-throughput screening). We lean, in contrast, to r*ational tuning* of E_B,[62, 94] which is based on an *educated* pre-selection of several candidates for efficient catalysts followed by a computational "testing". This approach *necessarily* requires understanding the mechanisms underlying the binding of an adsorbate to a substrate. These mechanisms nevertheless are quite complex, as we shall see below.

The formation of covalent and/or ionic bonds between an adsorbate and a substrate results from a valence charge density redistribution between the adsorbate and substrate. The formation of that local bond reduces the total energy of the system by E_{BF} (the bond-formation energy, the sum of the covalent- and ionic-bond formation energy), which in turn reflects bond strength. However, the above local charge redistribution necessarily induces an electronic density response from the rest of the substrate[75]. For example, for transition-metal substrates the charge density is redistributed in a quite extended surface and sub-surface region (see Fig. 3 in Ref.[75]). Naturally, this perturbation causes an *increase in the total energy of the system*, E_{elec}*. Next, the lattice is distorted to adjust to the perturbed charge density. This adjustment ("relaxation") partially compensates the energy increase caused by the extended electron density perturbation. Still, such lattice distortion also increases the total energy. This leaves us with an *effective* electronic and lattice-distortion energy increase E_{elec} and E_{rx} respectively. Thus, overall, the net perturbation increases the total energy by

$$E_{pert} = E_{elec} + E_{rx} \tag{5.1.98}$$

Hence, whenever E_{pert} is not negligible, one must recognize that,

$$E_B = E_{BF} + E_{per} \tag{5.1.99}$$

In regards to the so far known magnitude of E_{rx}, let us recall that two decades ago, it was estimated that E_{rx} for CO on transition metal surfaces is less than 0.05 eV[71]. Being that an inconsequential value, E_{rx} has not been considered in the design of catalysts until recently. Thus, contrary to Eq.(5.1.99), E_B has for the most part been assumed to exactly represent bond strength: $E_B = E_{BF}$ and, as a consequence, rational tuning of $E_B$has been

tackled through models addressing only the connection between bond strength, E_{BF}, and the electronic structure of potential catalyst surfaces[71]. Nevertheless, contrary to these premises and practices, recent studies show that E_{rx} is comparable to E_B for atomic oxygen adsorption on metal nanoparticles[106], and it is significant for other systems[75, 107-108]. For example, E_{rx} amounts up to 0.25 eV for Au(111) upon adsorption of atomic oxygen[75]. Clearly, E_{rx} cannot be neglected in such cases.

While E_{rx} has been obtained in various studies, to our knowledge, the total energy increase associated with the electronic perturbation (E_{elec}) was considered only very recently[75]. The electronic contribution to E_{pert} may be critical for catalytically relevant systems. For example, for oxygen adsorption on various transition metals surface, it has been found that E_{elec}, may be as high as 1 eV and varies significantly from metal to metal (1.25 eV for Au(111) and 0.87 eV for Ag(111))[75].

So far, our studies comparing E_{elec} and E_{rx} have shown larger contributions from E_{elec} than from E_{rx}. Nevertheless, notice that, because of the compensating character of the lattice distortion, the original electronic perturbation energy E_{elec}* can be larger than or equal to E_{rx}. Consequently, E_{elec} could be zero if E_{rx} totally compensates E_{elec}*.

The essential point, however, is that Eq.5.1.99 and the known values of E_{pert} so far[75] hint that rational tuning of E_B, and thus rational design of catalysts, may be a quite deceptive task unless we become aware of and reveal the factors controlling E_{elect} and E_{rx}, and not only focus on the aspects that determine bond strength. Until now, only a few steps have been made in the former direction[75, 106-108]. Further progress in understanding and tailoring E_{elect} and E_{rx} requires studying various potential catalysts with diverse properties,

in particular different electronic structures. Therefore, in this work, we investigate the perturbation effects on the binding energy of carbon monoxide (CO) and then hydroxide (OH) on metal-doped defected graphene. One reason for this choice is that a number of graphene-based materials, especially doped defected graphene, demonstrate promising catalytic properties[92-94, 109-118]. Indeed, pristine graphene is too inert to facilitate catalytic reactions, whereas dangling carbon bonds around vacancies make defected graphene too reactive for many reactions. Nonetheless, it has been shown[94, 113, 116] that anchoring a metal atom to a graphene vacancy may create adsorption sites of favorable catalytic reactivity. Next, since the electronic structure of doped graphene differs significantly from that of widely studied metal surface catalysts[94, 116], then one may expect new input into the causes and effects of the perturbation on the binding of adsorbates. Finally, CO and OH are selected as the adsorbates because they are involved in numerous catalytic reactions of high environmental and technological impact.

In this work, we study metal-doped graphene (M-Gr) systems in which a metal atom (M=Ru, Ir, Pd, Pt, Ag, Au) is incorporated into a 5–8–5 di-vacancy of a graphene (Fig.19). The reasons for this choice are: (a) This vacancy type is quite stable[119] and known to trap transition metal atoms[94, 120-121]. (b) The selected M-elements represent transition metals with varying number of *d*-electrons, and different magnitude of relativistic effects on *d*-bands, which is important for understanding the relationship between the electronic structure, E_{pert}, and E_{rx}.

5.2 **Computational Methods**

Our DFT-based total-energy calculations are performed using version 5.3 of the Vienna *Ab-initio* Software Package[66], projector augmented wave potentials[104], and the Perdew-Burke-Ernzerhof (PBE) parameterization[17] for the exchange and correlation functional. In order to model defected graphene by 5-8-5 di-vacancies (DV), we use a supercell that includes the defected graphene sheet with a single 5-8-5 DV sheet with a 4×4 in-plane periodicity and a ~14Å vacuum layer. Reciprocal-space integrations inside the Brillouin zone are performed using a (4×4×1) *k*-point mesh. Cutoff energies of 400 eV and 600 eV were set for the plane wave expansion of wave functions and charge density, respectively. The total-energy calculation for each configuration of the atomic positions is iterated until energy variations are below 10^{-6} eV. Based on this information, the total energy is minimized as a function of the atomic positions by reducing the Hellmann−Feynman forces[13] on either all or a selected set of atoms, in either all or selected directions, depending on the calculation (see text). Finally, the Xcrysden software[70] was used to visually represent geometric structures of the systems under consideration. We calculated the binding energy of the metal dopant atoms to the vacancy as:

$$E_B(M) = E_{tot}(M - Gr) - E_{tot}(Gr) - E_{tot}(M - at) \qquad (5.2.100)$$

where $E_{tot}(M\text{-}Gr)$, $E_{tot}(Gr)$, and $E_{tot}(M\text{-}at)$ are the total energies of the doped graphene, graphene with the di-vacancy, and the free metal atom, respectively. We also estimated the dopant formation energy as $E_{form}(M) = E_B(M) - E_{coh}(M)$, where $E_{coh}(M)$ is the cohesive energy of the bulk dopant element.

We calculated the CO and OH binding energies $E_B(CO)$ and $E_B(OH)$ as follows:

$$E_B(CO) = E_{tot}(M - Gr - CO) - E_{tot}(M - Gr) - E_{tot}(CO - mol) \quad (5.2.101)$$

$$E_B(OH) = E_{tot}(M - Gr - OH) - E_{tot}(M - Gr) - E_{tot}(OH - mol) \quad (5.2.102)$$

Here, $E_{tot}(M\text{-}Gr\text{-}CO)$, $E_{tot}(M\text{-}Gr)$, $E_{tot}(CO\text{-}mol)$ are the total energy of M-Gr adsorbed with CO, clean M-Gr, and a free CO molecule, and $E_{tot}(M\text{-}Gr\text{-}OH)$, $E_{tot}(M\text{-}Gr)$, $E_{tot}(OH\text{-}mol)$ are those of OH-molecule respectively.

In order to obtain E_{rx}, we take the relaxed *M-Gr-CO* structure, remove CO from it, calculate the total energy of the remaining structure (with frozen lattice), and subtract $E_{tot}(M\text{-}Gr)$ from it. The same procedure is applied in the case of OH too.

5.3 **Results and Discussion**

Regarding the binding of the metal dopant to the di-vacancy, we find that, for all dopants under consideration, the relaxed binding geometry is very similar in the following two aspects (See Fig.19): (1) metal atoms make four equivalent bonds with their neighboring carbon atoms (C_{NN}), and (2) all dopants take a slightly off-plane position. The dopants' binding energy ($E_{B(at)}$) and formation energy (E_{form}) (Table 12) indicate that (1) all dopants have a significant binding energy to the vacancy, and (2) doping is energetically preferable for all metals, except for Ag.

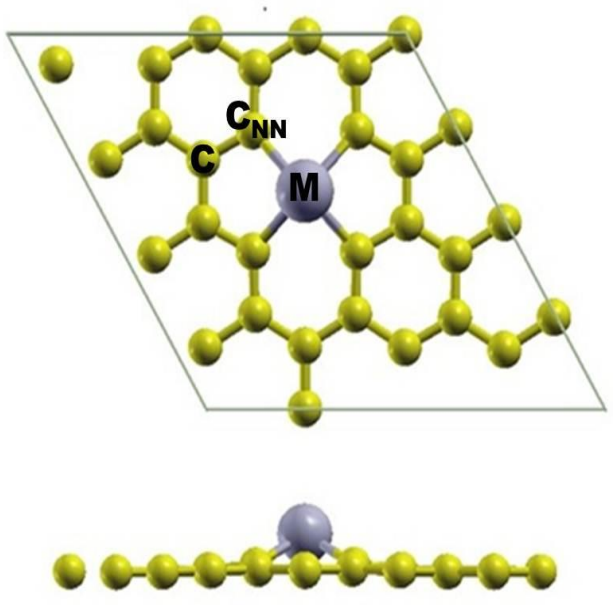

Figure 19: Calculated geometry of a Ru atom doping a 5–8–5 di-vacancy in graphene. M and CNN indicate the metal dopant and one of its nearest neighboring carbon atoms, respectively. C indicates one of the nearest neighbors of a CNN atom.

The calculations to study CO adsorption, the subject of interest of this work, were performed for the following adsorption sites: atop M, atop C_{NN} (C next to M) and atop C (that next to C_{NN}), as well as on bridges between these sites. In Table 13 we list the results for the preferred sites. Interestingly, for M=Ru and Ir in M-Gr, CO prefers to adsorb atop M; for M=Pd and Pt, CO prefers to adsorb at the M-C_{NN} bridge; whereas for M=Ag and Au, CO prefers to adsorb atop C_{NN}. One can thus conclude that Pd and Pt sites are less reactive than Ru and Ir ones, whereas Ag and Au sites are the least reactive among the selected M-sites in the M-Gr structures.

Table 12: Binding and formation energies of the dopants in a graphene 5 - 8 - 5 di-vacancy

Dopant	Ir	Ru	Pd	Pt	Ag	Au
$E_{B(at)}$ (eV)	-9.13	-8.68	-4.97	-7.49	-2.85	-4.56
E_{form} (eV)	-2.20	-1.92	-1.06	-1.63	0.10	-1.08

To rationalize this conclusion, one could simply use the notion that a higher local density of states (LDOS) around the Fermi level (E_F) of an adsorption site makes metals more reactive.

Table 13: Binding energies (E_B), lattice relaxation energies (E_{rx}), and their difference calculated for CO adsorption on M-Gr (E_B-E_{rx}) to estimate the CO - M-Gr bond-strength.

Dopant	**Ir**	**Ru**	**Pd**	**Pt**	**Ag**	**Au**
Preferred site	**atop Ir**	**atop Ru**	**Pd-C_{NN} bridge**	**Pt-C_{NN} bridge**	**C_{NN}**	**C_{NN}**
***E_B* (eV)**	-1.72	-1.37	-1.12	-1.04	-0.07	+0.18
***E_{rx}* (eV)**	0.16	0.14	1.05	1.02	0.92	0.91
***E_B*–*E_{rx}* (eV)**	-1.88	-1.51	-2.17	-2.06	-0.99	-0.73

Fig. 20 shows that, indeed, Ru has the highest *d*- LDOS around E_F, whereas Ag has the lowest one among M-Gr with M=Ru, Pt, and Ag, which would be consistent with the above ranking of the reactivity of the M-sites in the M-Gr structures.

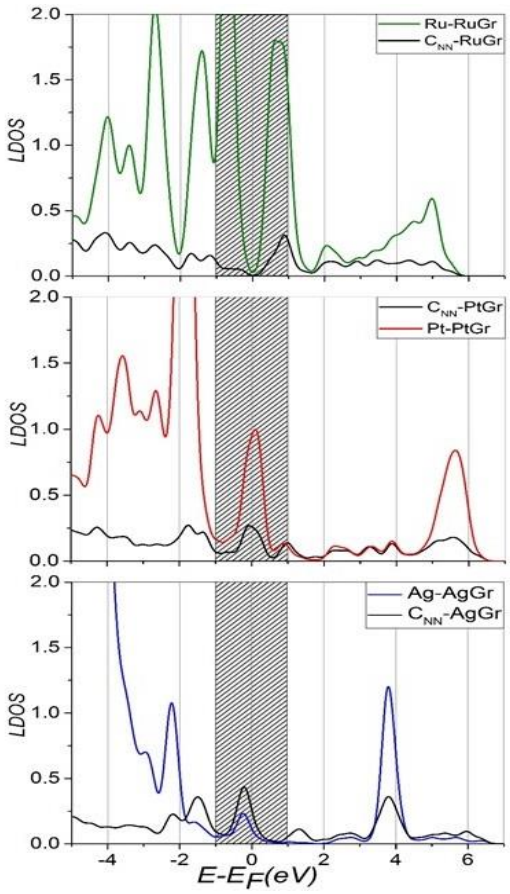

Figure 20: Metal d- and carbon (C_{NN}) p-LDOS calculated for Ru-Gr, Pt-Gr, and Ag-Gr. We highlight the energy region of ± 1 eV around E_F.

Let's see the case of OH.

Table 14: Binding energies (E_B), lattice relaxation energies (E_{rx}), and their difference calculated for OH adsorption on M-Gr (E_B-E_{rx}) to estimate the OH - M-Gr bond-strength.

Dopant	Ir	Ru	Pd	Pt	Ag	Au
Preferred adsorption site	atop Ir	atop Ru	Pd-C_{NN} bridge	Atop Pt	C_{NN}	C_{NN}
E_B (eV)	-4.01	-3.81	-2.52	-2.51	-2.96	-2.56
E_{rx} (eV)	0.21	0.10	0.88	0.46	1.13	1.04
E_B–E_{rx} (eV)	-4.22	-3.91	-3.40	-2.97	-4.09	-3.60

Table 14 also shows that the OH binding is stronger where C of graphene is involved. Conversely, the relaxation is higher in C-involved bindings.

However, the above rationale cannot explain the magnitude of E_B in general. E_B *(CO)* varies significantly from one M-Gr structure to another. Most strikingly, E_B *(CO)* is positive for Au-Gr. If one neglected the perturbation effect i.e., still assuming that $E_{BF} = E_B$, one could interpret, for example, that (1) CO makes the strongest bond (highest E_{BF}) with Ir-Gr, and, (2) no bond at all is formed between CO and Au-Gr, doubtful assessments that are the subject of the following discussion.

Indeed, if the perturbation effect is significant, one cannot neglect that, according to Eq. 5.1.99, E_{BF} is in fact given by:

$$E_{BF} = E_B - E_{pert} \tag{5.3.103}$$

The problem of applying Eq.(5.2.103) is that E_{pert} includes a contribution from excited electronic states, for which it has been a challenging problem to calculate it directly from first principles[75].

There is, however, one simple and preliminary way to estimate E_{pert}[75]. Namely, as discussed in the introduction, there is a relation between E_{pert} and E_{rx}: $E_{pert} \geq E_{rx}$, and E_{rx} can be accurately calculated within DFT, because it is defined for ground electronic states. We can thus use E_{rx} to determine the contribution of the lattice distortion to E_{pert} but also to estimate the lowest possible value of E_{BF}:

$$|E_{BF}| > |E_B - E_{rx}| \tag{5.3.104}$$

Table 13 shows that E_{rx} varies within a wide range depending on the metal dopant and reaches very high values (>1 eV) for some of them. To illustrate how unusually high these numbers are, one may compare them with other available E_{rx} values. For the transition metal surfaces considered in Ref. 70, the largest E_{rx} reported reaches 0.25 eV (for O on a 3×3 Au (111) supercell). Next, for a much larger O coverage (eight O atoms adsorbed on a Au_{79} cluster), which is expected to yield a huge perturbation, E_{rx} is lower than 1 eV per O atom[106]. Notice that in the latter case, there is one adsorbate per ~10 cluster atoms, whereas in our case there is one adsorbate per 31 M-Gr atoms. Furthermore, CO is expected to cause a smaller perturbation than O, because CO is less reactive than O. Indeed, we find that E_{rx} for O adsorption on Au-Gr is much larger (1.90 eV) than that for CO. Also, the comparison between Ir or Ru and Pd and Pt shows that CO is more strongly bound to Pd-Gr than to Ir-Gr, for example. Thus, once one takes into account the effect of the lattice

distortion on E_B, it is clear that E_B by itself may also fail at discerning which systems yield the strongest bonds.

Our results in Table 13 also show that, if CO adsorbs on a metal site, then E_{rx} is low, whereas if a graphene site is involved (M-Gr – C_{NN} bridge or C_{NN} adsorption sites) then E_{rx} is very large. The latter indicates that the unusually large E_{rx} is associated, not with the metal dopant itself, but with the response of the graphene lattice to the adsorption, which reveals *another unique property of graphene – its unusually strong lattice response on adsorption of an atom or molecule around dopant sites*.

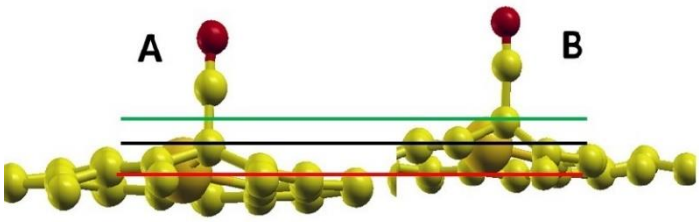

Figure 21: Geometries of CO adsorbed on the C_{NN} site of Au-Gr. A - geometry calculated for the equilibrium (relaxed) adsorption, B - geometry calculated for a CO position in the course of its desorption. Small yellow, large yellow and red balls represent carbon, gold and oxygen atoms, respectively. The red, black and green horizontal lines mark the z-positions of the fixed corner atoms in the supercell, C_{NN} site for the relaxed structure, and C_{NN} site for the structure in the course of desorption

Returning to the remarkable case of CO on Au-Gr, notice that a high E_{rx} yields a low E_B value. Au-Gr is the most interesting illustration of this effect because E_B (CO) is positive for this system (Table 13). If one applied the assumption that $E_B = E_{BF}$, then one would conclude that CO does not bind on Au-Gr whatsoever. However, we have clear evidence that a significant CO–Au-Gr bond is formed. Indeed, we have modeled CO desorption by lifting CO from its initial position by small steps (0.02 Å - 0.03Å, see Fig.21

and Fig. 22) while letting the M-Gr structure and O relax at each step. We found that during CO desorption, a significant lattice distortion takes place: CO pulls up the C_{NN} atom underneath (and neighboring C atoms). Clearly, the only explanation for that response is a significant CO–C_{NN} bond, as predicted by Eqs. 5.1.99 and 5.2.103.

To understand the relation between E_{pert} and the desorption activation barrier E_{desorp}, let us recall that an adsorbate desorbs when the adsorbate−substrate bond is broken. That requires a minimum energy equal to E_{BF}. Therefore, there exists an energy activation barrier for desorption. Importantly, we suggest that E_{desorp} *− measured from the relaxed bound state − must be equal in magnitude to the bond formation energy*: $E_{BF} = -E_{desorp}$. The key benefit of the latter identity is that, although calculating E_{pert} *directly* from first principles is a complex task,[5] one can obtain E_{pert} from two first principles calculations as (rewriting Eq. (5.2.104)):

$$E_{pert} = E_B + E_{desorp} \tag{5.3.105}$$

Desorption barriers can be easily and accurately obtained within DFT. However, calculating such barriers for these systems is not without obstacles. We find, for example, that for Pd-Gr the Pd–C_{NN} bond is broken during CO desorption. That costs some "extra" energy which biases the value of the barrier since the bond is restored after desorption. Also, in the Pt-Gr case, CO moves from the Pt–C_{NN} bridge site to Pt atop site during the desorption process, which results in two barriers.

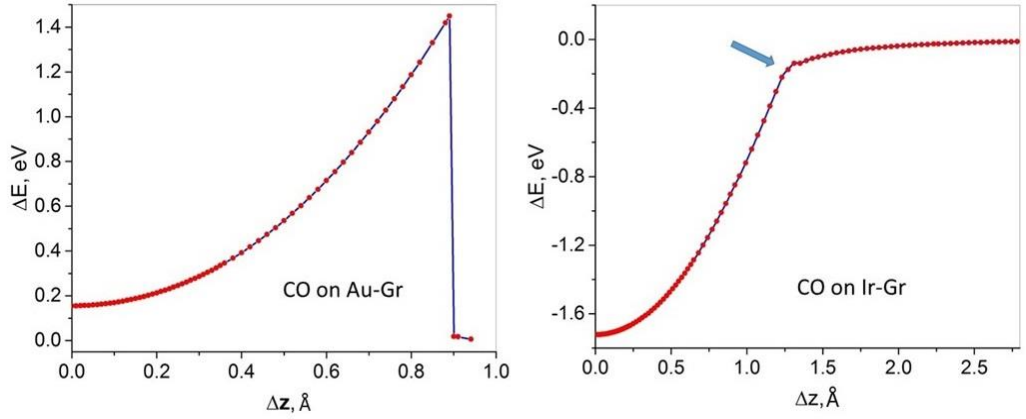

Figure 22: Calculated energy profiles of CO desorption for Au-Gr and Ir-Gr. ΔE =0 corresponds to the completely desorbed configuration: $E_{tot\_}$(CO free molecule) + E_{tot} (M-Gr); whereas Δ z = 0 corresponds to the distance between the C atom of CO and the C_{NN} atom (left) or the metal atom (right) when the M-Gr-CO structure is fully relaxed.

To avoid such shortcomings, we obtain E_{BF} and thus E_{pert} by calculating the desorption energy barrier while keeping the substrate's lattice frozen, E_{desorp}*, where E_{desorp}* = E_{desorp} + E_{rx}. Then, if E_B is known, one can correlate E_{BF}, E_{pert} and E_{rx} using the scheme in Fig. 23:

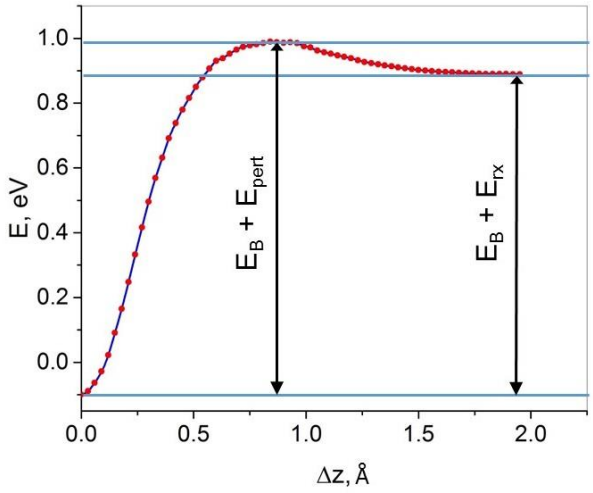

Figure 23: Energy profiles calculated for CO desorption from Ag-Gr, with the Ag-Gr lattice kept frozen. ΔE =0 corresponds to the completely desorbed configuration: E_{tot}(CO free molecule) + E_{tot} (M-Gr); Δz = 0 is for C of carbon – CNN distance for the relaxed adsorbed configuration.

$$E_{pert} = E_B + E_{desorp}{}^{*} - E_{rx} \qquad (5.3.106)$$

In agreement with the trend found for E_{rx}, the desorption barriers E_{desorp}* are large for those systems with high E_{rx}, and very low for systems for which E_{rx} is small. Table 15 displays the obtained values of E_{BF} and E_{pert} (See Eqs. 5.3.106 and 5.3.103) and clearly shows that taking into account E_{pert} may result in a dramatic deviation from the widely-used assumption that $E_B = E_{BF}$. Moreover, there is no linear or any other clear relation between these quantities.

Table 15: Perturbation energy (E_{pert}) and bond-formation energy (E_{BF}) calculated for CO adsorption on M-Gr. The corresponding binding energy (E_B) is provided as a reference and for comparison with E_{BF}:

Dopant	Ir	Ru	Pd	Pt	Ag	Au
Preferred adsorption site	atop Ir	atop Ru	Pd-C_{NN} bridge	Pt-C_{NN} bridge	C_{NN}	C_{NN}
E_{pert} (eV)	0.16	0.14	1.15	1.12	0.99	1.00
E_{BF} (eV)	-1.88	-1.51	-2.27	-2.16	-1.06	-0.82
E_B (eV)	-1.72	-1.37	-1.12	-1.04	-0.07	+0.18

Finally, notice that, in contrast to transition metal surfaces[75], E_{pert} in M-Gr does not exceed E_{rx} or not by much. The most plausible reason for this contrast is the great difference in the electronic structure of these systems: Transition metals have a large fraction of free-like electrons to screen that atoms get slightly ionized by the bond formation. Thus, the lattice is not distorted much and E_{rx} is much smaller than E_{elect}. The M-Gr structures, in contrast, do not have nearly as many free-like electrons to screen the charge transfer toward the bond. Thus, the bond-formation perturbation is relaxed mostly by distorting the lattice and E_{rx} turns out to be not much smaller than E_{elect}*. Besides, while M-Gr has very strong in-plane covalent C – C bonds, transition-metal bonds are typically weaker, hence, lattice distortions in M-Gr are typically energetically more expensive than those in transition metals. As for the carbon p_z-states in M-Gr, they do not overlap much for which their response to a perturbation is weak.

5.4 **Conclusion**

In conclusion, we have calculated binding energy E_B, lattice relaxation energy E_{rx} and desorption barriers E_{desorp} for CO on metal-doped graphene M-Gr, where M=Ru, Ir, Pd, Pt, Ag, Au. We find that E_{rx} varies significantly depending on the dopant and reaches unusually high values for some M-Gr systems. We also propose to use E_{desorp} to determine E_{pert}. Application of this approach to the M-Gr systems reveals substrates displaying large E_{pert}, thus demonstrating that *the widely used assumption that E_B represents bond strength totally fails.* Finally, knowledge of E_{pert} is very valuable, clearly not to determine the binding energy, but to break down the contributions to the binding energy, size their respective importance, rationalize the magnitude of the binding energy and extrapolate such knowledge to the rational design of materials.

CHAPTER 6 CONCLUSION

The main goal of this work is to find and demonstrate as much as possible advantage of rational design to predict promising electrocatalysts for the hydrogen fuel cell electrodes. The idea of the approach is to use existing knowledge to preselect the structures which may be thermodynamically and electrochemically stable and at the same time active toward reactions in question. This imply a selection of several candidate to promising catalyst (not hundreds as applied in very popular now computational screening approach). This selection is supposed to be made based on educative guess. Next, we "test" it computationally and narrow down the selection to one or two materials to provide it to experimentalists for actual testing. If it is about new materials, experiments: synthesizing, characterization and testing the properties of interest usually take a huge effort and time. Therefore it is important to provide to experimentalists a very good prediction to start (to convince them to start) the experimental work. Our results show that based on the educated guess we can predict very well the thermodynamic and electrochemical stability of the systems (mostly active monolayer on inexpensive substrate). It is harder to predict reactivity of the structure. It was recently believed that a number of simple models can easy predict the surface reactivity only by using the local densities of states of the catalyst surface atom. It appears, however that for the surfaces more complex than elemental metal surface these models fails. Nevertheless, we applied the ration design to preselect only a few candidate for hydrogen oxidation and oxygen reduction reactions on the hydrogen fuel cell electrodes and found that this approach works. We preselected three structure for hydrogen oxidation Pd/W(110), Ru/W(110), Au/W(110) . Our calculations have proven

that they are really stable and found that one of them (Pd/W(110) combines two important properties: the hydrogen oxidation is favorable on its surface and it has to be very tolerant to CO poisoning. Similarly, we preselected four candidates for the oxygen reduction reaction catalysts: AE/SE where AE = Pd, Pt and SE = Mo(110) and Nb(110). Based on our calculations we found that all of them have to be thermodynamically and electrochemically stable. The dissolution potential have to be higher than that of elemental Pt and Pd. Furthermore, our calculations of the ORR free energy diagrams suggest that Pt/Mo and Pt/ Nb have to have the ORR unset potential close to that of Pt. Needless to say that cost of the predicted material is much lower than that of Pt. Finally, considering that as we and other authors find that relation between the catalyst surface electronic structure and its reactivity is not clear and keeping in mind that binding energies of adsorbates are critical for the catalytic activity, we have focused on better understanding of the mechanisms underlying of binding of adsorbate to a surface. We focused on the effect of perturbation of the lattice upon binding and the energy (E_{pert}) attached to that (that was considered in 1970's but was ignored during the past two decades). We studied its effect on binding energy with an example of CO and OH binding on the metal doped graphene. We have found that the values of E_{pert} varies so much for different systems and may reach very high values (more than 1 eV) for some doped structures. This demonstrates that the widely used assumption that binding energy represents bond strength totally fails. This subject has not be studied much. Much work has to be done along this direction. But our results show that further work on it, further understanding of the relation between the material electronic structure and its perturbation energy has to be in focus of further

research and we believe that a progress in that will help to predict new efficient catalysts and better understand physics and chemistry of interaction between solid surfaces and adsorbates.

LIST OF REFERENECES

1. Atkens, P., *Physical Chemistry* 3ed.; W.H. Freeman and Company: New York, 1986.

2. Haile, S. M., Fuel cell materials and components☆☆. *Acta Materialia* **2003,** *51* (19), 5981-6000.

3. Kiejna, A.; Kresse, G.; Rogal, J.; De Sarkar, A.; Reuter, K.; Scheffler, M., Comparison of the full-potential and frozen-core approximation approaches to density-functional calculations of surfaces. *Physical Review B* **2006,** *73* (3), 035404.

4. Born, M.; Oppenheimer, R., Zur quantentheorie der molekeln. *Annalen der Physik* **1927,** *389* (20), 457-484.

5. Hartree, D. R. In *The wave mechanics of an atom with a non-Coulomb central field. Part I. Theory and methods*, Mathematical Proceedings of the Cambridge Philosophical Society, Cambridge Univ Press: 1928; pp 89-110.

6. Hartree, D. R. In *The wave mechanics of an atom with a non-Coulomb central field. Part II. Some results and discussion*, Mathematical Proceedings of the Cambridge Philosophical Society, Cambridge Univ Press: 1928; pp 111-132.

7. Slater, J. C., Note on Hartree's method. *Physical Review* **1930,** *35* (2), 210.

8. Fock, V., Näherungsmethode zur Lösung des quantenmechanischen Mehrkörperproblems. *Zeitschrift für Physik* **1930,** *61* (1-2), 126-148.

9. Fock, V., „Selfconsistent field “mit Austausch für Natrium. *Zeitschrift für Physik* **1930,** *62* (11-12), 795-805.

10. Hohenberg, P.; Kohn, W., Inhomogeneous Electron Gas. *Physical Review* **1964,** *136* (3B), B864-B871.

11. Kohanoff, J., *Electronic structure calculations for solids and molecules: theory and computational methods*. Cambridge University Press: 2006.

12. Kohn, W.; Sham, L., *Phys. Rev. B* **1965,** *15*, 2884-2901.

13. Payne, M. C.; Teter, M. P.; Allan, D. C.; Arias, T.; Joannopoulos, J., Iterative minimization techniques for ab initio total-energy calculations: molecular dynamics and conjugate gradients. *Reviews of Modern Physics* **1992,** *64* (4), 1045.

14. Wigner, E., Effects of the electron interaction on the energy levels of electrons in metals. *Transactions of the Faraday Society* **1938,** *34* (0), 678-685.

15. Ceperley, D. M.; Alder, B., Ground state of the electron gas by a stochastic method. *Physical Review Letters* **1980,** *45* (7), 566.

16. Jones, R. O.; Gunnarsson, O., The density functional formalism, its applications and prospects. *Reviews of Modern Physics* **1989,** *61* (3), 689-746.

17. Perdew, J. P.; Burke, K.; Ernzerhof, M., Generalized gradient approximation made simple. *Physical review letters* **1996,** *77* (18), 3865.

18. Ashcroft, N. W.; Mermin, N. D., Solid State Physics (Holt, Rinehart and Winston, New York, 1976). *Google Scholar* **2005**, 403.

19. Chadi, D. J.; Cohen, M. L., Special Points in the Brillouin Zone. *Physical Review B* **1973,** *8* (12), 5747-5753.

20. Phillips, J. C., Energy-band interpolation scheme based on a pseudopotential. *Physical Review* **1958,** *112* (3), 685.

21. Cohen, M. L.; Heine, V., The fitting of pseudopotentials to experimental data and their subsequent application. *Solid state physics* **1970,** *24*, 37-248.

22. Yin, M.; Cohen, M. L., Theory of ab initio pseudopotential calculations. *Physical review B* **1982,** *25* (12), 7403.

23. Sholl, D.; Steckel, J. A., *Density functional theory: a practical introduction*. John Wiley & Sons: 2011.

24. Hammer, B.; Nørskov, J. K., Theoretical surface science and catalysis—calculations and concepts. *Advances in catalysis* **2000,** *45*, 71-129.

25. Henkelman, G.; Arnaldsson, A.; Jónsson, H., A fast and robust algorithm for Bader decomposition of charge density. *Computational Materials Science* **2006,** *36* (3), 354-360.

26. Bader, R. F., *Atoms in molecules*. Wiley Online Library: 1990.

27. Tang, W.; Sanville, E.; Henkelman, G., A grid-based Bader analysis algorithm without lattice bias. *Journal of Physics: Condensed Matter* **2009,** *21* (8), 084204.

28. Laidler, K. J.; King, M. C., Development of transition-state theory. *The Journal of physical chemistry* **1983,** *87* (15), 2657-2664.

29. Cedillo, A., Density functional theory models of reactivity based on an energetic criterion. *Theoretical and Computational Chemistry* **2007,** *19*, 19-30.

30. Götz, M.; Wendt, H., Binary and ternary anode catalyst formulations including the elements W, Sn and Mo for PEMFCs operated on methanol or reformate gas. *Electrochimica Acta* **1998,** *43* (24), 3637-3644.

31. Korotkikh, O.; Farrauto, R., Selective catalytic oxidation of CO in H 2: fuel cell applications. *Catalysis Today* **2000,** *62* (2), 249-254.

32. Lemons, R. A., Fuel cells for transportation. *Journal of Power Sources* **1990,** *29* (1-2), 251-264.

33. Gasteiger, H. A.; Markovic, N.; Ross Jr, P. N.; Cairns, E. J., Carbon monoxide electrooxidation on well-characterized platinum-ruthenium alloys. *The Journal of Physical Chemistry* **1994,** *98* (2), 617-625.

34. Ralph, T.; Hogarth, M., Catalysis for low temperature fuel cells. *Platinum Metals Review* **2002,** *46* (3), 117-135.

35. Ishikawa, Y.; Liao, M.-S.; Cabrera, C. R., Oxidation of methanol on platinum, ruthenium and mixed Pt–M metals (M= Ru, Sn): a theoretical study. *Surface Science* **2000,** *463* (1), 66-80.

36. Igarashi, H.; Fujino, T.; Zhu, Y.; Uchida, H.; Watanabe, M., CO tolerance of Pt alloy electrocatalysts for polymer electrolyte fuel cells and the detoxification mechanism. *Physical Chemistry Chemical Physics* **2001,** *3* (3), 306-314.

37. Pereira, L. G. S.; Paganin, V. A.; Ticianelli, E. A., Investigation of the CO tolerance mechanism at several Pt-based bimetallic anode electrocatalysts in a PEM fuel cell. *Electrochimica Acta* **2009,** *54* (7), 1992-1998.

38. Ehteshami, S. M. M.; Chan, S. H., A review of electrocatalysts with enhanced CO tolerance and stability for polymer electrolyte membarane fuel cells. *Electrochimica Acta* **2013,** *93*, 334-345.

39. Garcia, A. C.; Paganin, V. A.; Ticianelli, E. A., CO tolerance of PdPt/C and PdPtRu/C anodes for PEMFC. *Electrochimica Acta* **2008,** *53* (12), 4309-4315.

40. Brankovic, S.; Wang, J.; Adžić, R., Pt submonolayers on Ru nanoparticles: a novel low Pt loading, high CO tolerance fuel cell electrocatalyst. *Electrochemical and Solid-State Letters* **2001,** *4* (12), A217-A220.

41. Brankovic, S.; Wang, J.; Zhu, Y.; Sabatini, R.; McBreen, J.; Adžić, R., Electrosorption and catalytic properties of bare and Pt modified single crystal and nanostructured Ru surfaces. *Journal of Electroanalytical Chemistry* **2002,** *524*, 231-241.

42. Ortigoza, M. A.; Stolbov, S.; Rahman, T. S., Formation of Pt islets on facets of Ru nanoparticles: First-principles study. *Physical Review B* **2008,** *78* (19), 195417.

43. Stolbov, S.; Ortigoza, M. A.; Adzic, R.; Rahman, T. S., High CO tolerance of Pt/Ru nanocatalyst: insight from first principles calculations. *The Journal of chemical physics* **2009,** *130* (12), 124714.

44. Hsieh, Y.-C.; Zhang, Y.; Su, D.; Volkov, V.; Si, R.; Wu, L.; Zhu, Y.; An, W.; Liu, P.; He, P., Ordered bilayer ruthenium–platinum core-shell nanoparticles as carbon monoxide-tolerant fuel cell catalysts. *Nature communications* **2013,** *4*.

45. Alayoglu, S.; Nilekar, A. U.; Mavrikakis, M.; Eichhorn, B., Ru–Pt core–shell nanoparticles for preferential oxidation of carbon monoxide in hydrogen. *Nature materials* **2008,** *7* (4), 333-338.

46. Petrii, O. A., Pt–Ru electrocatalysts for fuel cells: a representative review. *Journal of Solid State Electrochemistry* **2008,** *12* (5), 609-642.

47. Dai, Y.; Liu, Y.; Chen, S., Pt–W bimetallic alloys as CO-tolerant PEMFC anode catalysts. *Electrochimica Acta* **2013,** *89*, 744-748.

48. Wang, D.; Subban, C. V.; Wang, H.; Rus, E.; DiSalvo, F. J.; Abruña, H. D., Highly stable and CO-tolerant Pt/Ti0. 7W0. 3O2 electrocatalyst for proton-exchange membrane fuel cells. *Journal of the American Chemical Society* **2010,** *132* (30), 10218-10220.

49. Kwon, K.; Jin, S.-a.; Lee, K. H.; You, D. J.; Pak, C., Performance enhancement of Pd-based hydrogen oxidation catalysts using tungsten oxide. *Catalysis Today* **2014,** *232*, 175-178.

50. Maillard, F.; Peyrelade, E.; Soldo-Olivier, Y.; Chatenet, M.; Chaînet, E.; Faure, R., Is carbon-supported Pt-WO x composite a CO-tolerant material? *Electrochimica acta* **2007,** *52* (5), 1958-1967.

51. Pereira, L. G. S.; dos Santos, F. R.; Pereira, M. E.; Paganin, V. A.; Ticianelli, E. A., CO tolerance effects of tungsten-based PEMFC anodes. *Electrochimica acta* **2006,** *51* (19), 4061-4066.

52. Shim, J.; Lee, C.-R.; Lee, H.-K.; Lee, J.-S.; Cairns, E. J., Electrochemical characteristics of Pt–WO 3/C and Pt–TiO 2/C electrocatalysts in a polymer electrolyte fuel cell. *Journal of Power Sources* **2001,** *102* (1), 172-177.

53. Park, K.-W.; Ahn, K.-S.; Choi, J.-H.; Nah, Y.-C.; Kim, Y.-M.; Sung, Y.-E., Pt-WOx electrode structure for thin-film fuel cells. *Applied physics letters* **2002,** *81* (5), 907-909.

54. Cui, X.; Guo, L.; Cui, F.; He, Q.; Shi, J., Electrocatalytic activity and CO tolerance properties of mesostructured Pt/WO3 composite as an anode catalyst for PEMFCs. *The Journal of Physical Chemistry C* **2009,** *113* (10), 4134-4138.

55. Hassan, A.; Paganin, V. A.; Carreras, A.; Ticianelli, E. A., Molybdenum carbide-based electrocatalysts for CO tolerance in proton exchange membrane fuel cell anodes. *Electrochimica Acta* **2014,** *142*, 307-316.

56. Schmidt, T.; Jusys, Z.; Gasteiger, H.; Behm, R.; Endruschat, U.; Boennemann, H., On the CO tolerance of novel colloidal PdAu/carbon electrocatalysts. *Journal of Electroanalytical Chemistry* **2001,** *501* (1), 132-140.

57. Kibler, L.; El-Aziz, A.; Kolb, D., Electrochemical behaviour of pseudomorphic overlayers: Pd on Au (1 1 1). *Journal of Molecular Catalysis A: Chemical* **2003,** *199* (1), 57-63.

58. Pluntke, Y.; Kibler, L.; Kolb, D., Unique activity of Pd monomers: hydrogen evolution at AuPd (111) surface alloys. *Physical Chemistry Chemical Physics* **2008,** *10* (25), 3684-3688.

59. Al-Odail, F. A.; Anastasopoulos, A.; Hayden, B. E., The hydrogen evolution reaction and hydrogen oxidation reaction on thin film PdAu alloy surfaces. *Physical Chemistry Chemical Physics* **2010,** *12* (37), 11398-11406.

60. Liu, P.; Nørskov, J. K., Ligand and ensemble effects in adsorption on alloy surfaces. *Physical Chemistry Chemical Physics* **2001,** *3* (17), 3814-3818.

61. Maroun, F.; Ozanam, F.; Magnussen, O.; Behm, R., The role of atomic ensembles in the reactivity of bimetallic electrocatalysts. *Science* **2001,** *293* (5536), 1811-1814.

62. Stolbov, S.; Alcántara Ortigoza, M., Rational design of competitive electrocatalysts for hydrogen fuel cells. *The journal of physical chemistry letters* **2012,** *3* (4), 463-467.

63. Barbir, F., *PEM fuel cells: theory and practice*. Academic Press: 2013.

64. Liu, P.; Nørskov, J. K., Kinetics of the anode processes in PEM fuel cells–the promoting effect of Ru in PtRu anodes. *Fuel Cells* **2001,** *1* (3-4), 192-201.

65. Liu, P.; Logadottir, A.; Nørskov, J. K., Modeling the electro-oxidation of CO and H 2/CO on Pt, Ru, PtRu and Pt 3 Sn. *Electrochimica Acta* **2003,** *48* (25), 3731-3742.

66. Kresse, G.; Furthmüller, J., Efficiency of ab-initio total energy calculations for metals and semiconductors using a plane-wave basis set. *Computational Materials Science* **1996,** *6* (1), 15-50.

67. Tan, X.; Zhou, J.; Peng, Y., First-principles study of oxygen adsorption on Fe(1 1 0) surface. *Applied Surface Science* **2012,** *258* (22), 8484-8491.

68. Cox, J.; Wagman, D. D.; Medvedev, V. A., *CODATA key values for thermodynamics*. Chem/Mats-Sci/E: 1989.

69. Nørskov, J. K.; Rossmeisl, J.; Logadottir, A.; Lindqvist, L.; Kitchin, J. R.; Bligaard, T.; Jonsson, H., Origin of the overpotential for oxygen reduction at a fuel-cell cathode. *The Journal of Physical Chemistry B* **2004,** *108* (46), 17886-17892.

70. Kokalj, A., Computer graphics and graphical user interfaces as tools in simulations of matter at the atomic scale. *Computational Materials Science* **2003,** *28* (2), 155-168.

71. Hammer, B.; Morikawa, Y.; Nørskov, J. K., CO chemisorption at metal surfaces and overlayers. *Physical review letters* **1996,** *76* (12), 2141.

72. Nørskov, J. K.; Abild-Pedersen, F.; Studt, F.; Bligaard, T., Density functional theory in surface chemistry and catalysis. *Proceedings of the National Academy of Sciences* **2011,** *108* (3), 937-943.

73. Stolbov, S.; Zuluaga, S., Factors controlling the reactivity of catalytically active monolayers on metal substrates. *The journal of physical chemistry letters* **2013,** *4* (9), 1537-1540.

74. Nørskov, J. K.; Bligaard, T.; Rossmeisl, J.; Christensen, C. H., Towards the computational design of solid catalysts. *Nature chemistry* **2009,** *1* (1), 37-46.

75. Ortigoza, M. A.; Stolbov, S., The perturbation energy: A missing key to understand the "nobleness" of bulk gold. *The Journal of chemical physics* **2015,** *142* (19), 194705.

76. Ortigoza, M. A.; Rahman, T. S.; Heid, R.; Bohnen, K.-P., Ab initio calculations of the dispersion of surface phonons of ac (2× 2) CO overlayer on Ag (001). *Journal of Physics: Condensed Matter* **2010,** *22* (39), 395001.

77. Singh-Miller, N. E.; Marzari, N., Surface energies, work functions, and surface relaxations of low-index metallic surfaces from first principles. *Physical Review B* **2009,** *80* (23), 235407.

78. Da Silva, J. L.; Stampfl, C.; Scheffler, M., Converged properties of clean metal surfaces by all-electron first-principles calculations. *Surface science* **2006,** *600* (3), 703-715.

79. Hulse, J.; Küppers, J.; Wandelt, K.; Ertl, G., UV-Photoelectron spectroscopy from xenon adsorbed on heterogeneous metal surfaces. *Applications of Surface Science* **1980,** *6* (3-4), 453-463.

80. Kubiak, G. D., Two-photon photoelectron spectroscopy of Pd (111). *Journal of Vacuum Science & Technology A* **1987,** *5* (4), 731-734.

81. Vielstich, W.; Yokokawa, H.; Gasteiger, H. A., *Handbook of fuel cells: fundamentals technology and applications*. John Wiley & Sons: 2009.

82. Adzic, R.; Zhang, J.; Sasaki, K.; Vukmirovic, M.; Shao, M.; Wang, J.; Nilekar, A., Mavrikakis, JA Valerio, F. Uribe. *Topics in Catalysis* **2007,** *46*, 249.

83. Gong, K.; Chen, W.-F.; Sasaki, K.; Su, D.; Vukmirovic, M. B.; Zhou, W.; Izzo, E. L.; Perez-Acosta, C.; Hirunsit, P.; Balbuena, P. B., Platinum-monolayer electrocatalysts: palladium interlayer on IrCo alloy core improves activity in oxygen-reduction reaction. *Journal of Electroanalytical Chemistry* **2010,** *649* (1), 232-237.

84. Nilekar, A. U.; Mavrikakis, M., Improved oxygen reduction reactivity of platinum monolayers on transition metal surfaces. *Surface Science* **2008,** *602* (14), L89-L94.

85. Zhang, J.; Vukmirovic, M. B.; Xu, Y.; Mavrikakis, M.; Adzic, R. R., Controlling the Catalytic Activity of Platinum-Monolayer Electrocatalysts for Oxygen Reduction with Different Substrates. *Angewandte Chemie International Edition* **2005,** *44* (14), 2132-2135.

86. Zhou, W. P.; Yang, X.; Vukmirovic, M. B.; Koel, B. E.; Jiao, J.; Peng, G.; Mavrikakis, M.; Adzic, R. R., Improving electrocatalysts for O(2) reduction by fine-tuning the Pt-support interaction: Pt monolayer on the surfaces of a Pd(3)Fe(111) single-crystal alloy. *J Am Chem Soc* **2009,** *131* (35), 12755-62.

87. Zuluaga, S.; Stolbov, S., Factors controlling the energetics of the oxygen reduction reaction on the Pd-Co electro-catalysts: Insight from first principles. *The Journal of chemical physics* **2011,** *135* (13), 134702.

88. Wang, C.; Van der Vliet, D.; More, K. L.; Zaluzec, N. J.; Peng, S.; Sun, S.; Daimon, H.; Wang, G.; Greeley, J.; Pearson, J., Multimetallic Au/FePt3 nanoparticles as highly durable electrocatalyst. *Nano Letters* **2010,** *11* (3), 919-926.

89. Zhang, L.; Iyyamperumal, R.; Yancey, D. F.; Crooks, R. M.; Henkelman, G., Design of Pt-shell nanoparticles with alloy cores for the oxygen reduction reaction. *ACS nano* **2013,** *7* (10), 9168-9172.

90. Wang, S.; Yu, D.; Dai, L.; Chang, D. W.; Baek, J.-B., Polyelectrolyte-functionalized graphene as metal-free electrocatalysts for oxygen reduction. *ACS nano* **2011,** *5* (8), 6202-6209.

91. Yu, D.; Zhang, Q.; Dai, L., Highly efficient metal-free growth of nitrogen-doped single-walled carbon nanotubes on plasma-etched substrates for oxygen reduction. *Journal of the American Chemical Society* **2010,** *132* (43), 15127-15129.

92. Zhang, L.; Xia, Z., Mechanisms of oxygen reduction reaction on nitrogen-doped graphene for fuel cells. *The Journal of Physical Chemistry C* **2011,** *115* (22), 11170-11176.

93. Chen, X.; Chen, S.; Wang, J., Screening of catalytic oxygen reduction reaction activity of metal-doped graphene by density functional theory. *Applied Surface Science* **2016,** *379*, 291-295.

94. Stolbov, S.; Ortigoza, M. A., Gold-doped graphene: A highly stable and active electrocatalysts for the oxygen reduction reaction. *The Journal of chemical physics* **2015,** *142* (15), 154703.

95. Allendorf, M. D., Oxygen reduction reaction: A framework for success. *NATURE ENERGY* **2016,** *1*, 1-2.

96. Miner, E. M.; Fukushima, T.; Sheberla, D.; Sun, L.; Surendranath, Y.; Dincă, M., Electrochemical oxygen reduction catalysed by Ni3 (hexaiminotriphenylene) 2. *Nature communications* **2016,** *7*.

97. Sheberla, D.; Sun, L.; Blood-Forsythe, M. A.; Er, S. l.; Wade, C. R.; Brozek, C. K.; Aspuru-Guzik, A. n.; Dincă, M., High electrical conductivity in Ni3 (2, 3, 6, 7, 10, 11-hexaiminotriphenylene) 2, a semiconducting metal–organic graphene analogue. *Journal of the American Chemical Society* **2014,** *136* (25), 8859-8862.

98. Zhou, M.; Wang, H.-L.; Guo, S., Towards high-efficiency nanoelectrocatalysts for oxygen reduction through engineering advanced carbon nanomaterials. *Chemical Society Reviews* **2016,** *45* (5), 1273-1307.

99. Lide, D. R., *CRC handbook of chemistry and physics*. CRC press: 2004; Vol. 85.

100. Greeley, J.; Nørskov, J. K., Electrochemical dissolution of surface alloys in acids: Thermodynamic trends from first-principles calculations. *Electrochimica Acta* **2007,** *52* (19), 5829-5836.

101. Nawaz, Z.; Alqahtani, A.; Baksh, F.; Naveed, R., *Rational asymmetric catalyst design, intensification and modeling*. Citeseer: 2012.

102. Adzic, R., Frontiers in electrochemistry. *Electrocatalysis* **1998,** *5*, 197.

103. Li, X.; Huang, Q.; Zou, Z.; Xia, B.; Yang, H., Low temperature preparation of carbon-supported Pd Co alloy electrocatalysts for methanol-tolerant oxygen reduction reaction. *Electrochimica Acta* **2008,** *53* (22), 6662-6667.

104. Kresse, G.; Joubert, D., From ultrasoft pseudopotentials to the projector augmented-wave method. *Physical Review B* **1999,** *59* (3), 1758.

105. Stolbov, S.; Ortigoza, M. A., Rational catalyst design methodologies – Principles and factors affecting the catalyst design. 2017.

106. Lu, C.-Y.; Henkelman, G., Role of geometric relaxation in oxygen binding to metal nanoparticles. *The journal of physical chemistry letters* **2011,** *2* (11), 1237-1240.

107. Wang, X.-G.; Fisher, G. B., Phase diagram of molecular oxygen adsorption on the (111) platinum surface. *Physical review letters* **2007,** *99* (6), 066101.

108. Hoft, R. C.; Ford, M. J.; McDonagh, A. M.; Cortie, M. B., Adsorption of amine compounds on the Au (111) surface: a density functional study. *The Journal of Physical Chemistry C* **2007,** *111* (37), 13886-13891.

109. Jiao, Y.; Zheng, Y.; Jaroniec, M.; Qiao, S. Z., Origin of the electrocatalytic oxygen reduction activity of graphene-based catalysts: a roadmap to achieve the best performance. *Journal of the American Chemical Society* **2014,** *136* (11), 4394-4403.

110. Byon, H. R.; Suntivich, J.; Shao-Horn, Y., Graphene-based non-noble-metal catalysts for oxygen reduction reaction in acid. *Chemistry of Materials* **2011,** *23* (15), 3421-3428.

111. Kattel, S.; Wang, G., Reaction pathway for oxygen reduction on FeN4 embedded graphene. *The journal of physical chemistry letters* **2014,** *5* (3), 452-456.

112. Studt, F., The oxygen reduction reaction on nitrogen-doped graphene. *Catalysis letters* **2013,** *143* (1), 58-60.

113. Kaukonen, M.; Krasheninnikov, A.; Kauppinen, E.; Nieminen, R., Doped graphene as a material for oxygen reduction reaction in hydrogen fuel cells: a computational study. *ACS Catalysis* **2013,** *3* (2), 159-165.

114. Liang, W.; Chen, J.; Liu, Y.; Chen, S., Density-functional-theory calculation analysis of active sites for four-electron reduction of O2 on Fe/N-doped graphene. *ACS Catalysis* **2014,** *4* (11), 4170-4177.

115. Wang, W. L.; Santos, E. J.; Jiang, B.; Cubuk, E. D.; Ophus, C.; Centeno, A.; Pesquera, A.; Zurutuza, A.; Ciston, J.; Westervelt, R., Direct observation of a long-lived single-atom catalyst chiseling atomic structures in graphene. *Nano letters* **2014,** *14* (2), 450-455.

116. Tang, Y.; Yang, Z.; Dai, X., A theoretical simulation on the catalytic oxidation of CO on Pt/graphene. *Physical Chemistry Chemical Physics* **2012,** *14* (48), 16566-16572.

117. Yoo, E.; Okada, T.; Akita, T.; Kohyama, M.; Honma, I.; Nakamura, J., Sub-nano-Pt cluster supported on graphene nanosheets for CO tolerant catalysts in polymer electrolyte fuel cells. *Journal of power sources* **2011,** *196* (1), 110-115.

118. Park, J.-e.; Jang, Y. J.; Kim, Y. J.; Song, M.-s.; Yoon, S.; Kim, D. H.; Kim, S.-J., Sulfur-doped graphene as a potential alternative metal-free electrocatalyst and Pt-catalyst supporting material for oxygen reduction reaction. *Physical Chemistry Chemical Physics* **2014,** *16* (1), 103-109.

119. Krasheninnikov, A.; Nieminen, R., Attractive interaction between transition-metal atom impurities and vacancies in graphene: a first-principles study. *Theoretical Chemistry Accounts* **2011,** *129* (3-5), 625-630.

120. Malola, S.; Häkkinen, H.; Koskinen, P., Gold in graphene: in-plane adsorption and diffusion. *Applied Physics Letters* **2009,** *94* (4), 043106.

121. Zhang, W.; Sun, L.; Xu, Z.; Krasheninnikov, A. V.; Huai, P.; Zhu, Z.; Banhart, F., Migration of gold atoms in graphene ribbons: Role of the edges. *Physical Review B* **2010,** *81* (12), 125425.